

1 **Title**

2 **Beyond Volume: Unraveling the Genetics of Human Brain Geometry**

3 **Authors**

5 Sabrina A. Primus^{1,2,3}, Felix Hoffstaedter^{4,5}, Federico Raimondo^{4,5}, Simon B. Eickhoff^{4,5},
6 Juliane Winkelmann^{1,3,6,7}, Konrad Oexle^{1,2,3,†,*}, Kaustubh R. Patil^{4,5,†,*}

7
8 Email of corresponding authors: konrad.oexle@helmholtz-munich.de, k.patil@fz-
9 juelich.de

10
11 **Affiliations**

14 1 Institute of Neurogenomics, Helmholtz Zentrum München, German Research Center for
15 Environmental Health, Neuherberg, Germany.

16 2 Neurogenetic Systems Analysis Group, Institute of Neurogenomics, Helmholtz Zentrum
17 München, German Research Center for Environmental Health, Neuherberg, Germany.

18 3 Institute of Human Genetics, TUM School of Medicine and Health, Technical
19 University of Munich, Munich, Germany.

20 4 Institute of Neuroscience and Medicine, Brain & Behaviour (INM-7), Research Centre
21 Jülich, Jülich, Germany.

22 5 Institute of Systems Neuroscience, Medical Faculty, Heinrich Heine University
23 Düsseldorf, Düsseldorf, Germany.

24 6 Munich Cluster for Systems Neurology (SyNergy), Munich, Germany.

25 7 German Center for Mental Health (DZPG), partner site Munich–Augsburg, Munich–
26 Augsburg, Germany.

27
28 † These authors contributed equally to this work.

29
30 **Abstract**

32 Brain geometry impacts brain function. A quantitative encoding of form is provided by the
33 Laplace-Beltrami operator's spectrum of eigenvalues (LBS). We examined LBS genetics of 22
34 subcortical brain structures including cerebellum in 19,862 healthy White-British UK Biobank
35 participants by multivariate GWAS (MOSTest) on the first 49 eigenvalues each. Controlling for
36 surface and volume, we identified 80 unique variants ($p<1/22*5E-8$) influencing the shapes of
37 one or several structures, with the highest yield (37 variants) for brain stem. The previously
38 known influence of several of these loci on basic morphology, such as volume, is thus shown to
39 also influence complex shape. Known associations of observed loci with blood pressure,
40 neurodegeneration, alcohol consumption, and mental disorders hint at preclinical stages of these
41 conditions potentially mediating the genetic effect on brain morphology. Significant correlations
42 between LBS of several brain structures and the polygenic risks of hypertension, ischemic stroke
43 and schizophrenia evince brain shapes as early biomarkers.

44
45 **Teaser**

46 Multivariate association study reveals genetic basis of detailed brain shape beyond volume
47 and possible relations to neurodegenerative diseases.

50 **MAIN TEXT**

51

52 **Introduction**

53 The human brain comprises an intricate constellation of diverse substructures, each of
54 which has specific functions and forms complex interactions with other parts of the brain.
55 Investigating the morphological properties of these substructures and deciphering their genetic
56 underpinnings is imperative for advancing our understanding of the human brain in health and
57 disease. Previous genetic studies have investigated crude parameters such as volume and surface
58 area (1–5). The genetics of the intricate shapes of brain structures remain largely unexamined,
59 however, representing a gap in comprehensive understanding of brain anatomy.

60 The structures within the human brain exhibit a range of shapes, from the more spherical
61 amygdala to the elongated hippocampus. Basic metrics such as volume and surface area do not
62 adequately capture the nuanced details of these shapes and thus fall short of providing a sufficient
63 description of their morphology. There is evidence for a high inter-individual variance in these
64 intricate details, with a substantial proportion being heritable (6–8). Initial efforts to delve into the
65 genetic underpinning of this heritable aspect used techniques like voxel-based analysis in
66 combination with dimension reduction methods (9, 10), or global-to-local representations of brain
67 shapes (11, 12). Each of these techniques carries its own challenges, including reduced robustness
68 and accuracy due to suboptimal image registration, high computational effort, or a lack of
69 physical interpretability due to dimensionality reduction or a prohibitive dimensionality of image-
70 derived features.

71 The Laplace-Beltrami operator provides a multivariate spectral representation of a shape,
72 capturing its characteristics in detail (13, 14). The Laplace-Beltrami spectrum (LBS), a set of
73 ordered eigenvalues, is obtained by solving the Helmholtz equation, a time-independent form of
74 the wave equation, on a Riemannian manifold which can be the surface of a given brain structure.
75 Solutions are decomposed into eigenfunctions (also referred to as “eigenmodes”) and their
76 corresponding eigenvalues representing the natural vibrations and their squared frequencies,
77 respectively, on the manifold underlying the shape, akin to the harmonic frequencies of the
78 membrane of a drum. Each sound or other vibration of a membrane can be represented as a
79 weighted sum of its eigenmodes, relating closely to the theory of spectral analysis in Fourier
80 series. Necessarily, the eigenmodes are strongly linked to a shape’s geometry, as visualized in a
81 seminal experiment by Ernst Chladni using vibrating plates (15). It has been asked since then
82 whether a shape can be represented by a unique series of eigenvalues or, metaphorically, whether
83 the shape of a drum can be heard (16). While the answer is affirmative for one-dimensional
84 shapes whose lengths are made audible by the harmonics or pure tones of string instruments, for
85 instance, this is not true in general for shapes with more than one dimension as there exist
86 isospectral shapes (17). Nevertheless, the known counterexamples appear to be rare (13) and
87 under certain symmetry assumptions, a unique assignment is possible (18). Consequentially, a
88 relatively small subsequence (e.g. 50 eigenvalues) of the increasingly ordered spectrum contains
89 enough geometric information to uniquely describe a shape by adequately capturing its curvatures
90 (13, 19–21), although the spectrum usually contains an infinite number of eigenvalues. Following
91 Ge et al. (6), we refer to this subsequence as the LBS (also known as Shape-DNA (13)). This
92 multidimensional intrinsic shape representation, as an isometric invariant, is independent of
93 rotation, translation, and scaling of the coordinate system, eliminating the need for error-prone
94 inter-individual image registration (22), and behaves continuously with any change in the
95 manifold. Recently, there is considerable interest in using geometric eigenmodes to explain
96 shape-associated biological mechanisms (23). The LBS appears to be a more straightforward
97 shape descriptor, however, which is computed efficiently (21) and thus well suited for large-scale

98 genome-wide association studies (GWASs) which require a quantitative representation of the
99 shape of brain structures at the individual level.

100 By performing GWAS, we aimed to reveal information on gene loci contributing to the
101 heritability of brain morphology as quantified by LBS. We derived the LBSs of 22 different brain
102 structures from a large MRI dataset provided by the UK Biobank (UKB). To reveal shape-specific
103 signals, we controlled for global characteristics such as brain volume and surface area. Since all
104 eigenvalues in an LBS contribute to the description of the respective shape, it is important to
105 study them jointly while accounting for their mutual dependencies. To achieve this, we employed
106 the state-of-the-art multivariate GWAS tool MOSTest (2), which accounts for the pairwise
107 correlations between eigenvalues and, by considering their joint distribution, has increased power
108 for detecting genetic associations. Our study focused on subcortical structures, brain stem and
109 cerebellum, in keeping with several studies which studied the genetics of their volumes (2, 5, 24–
110 26). These parts of the brain are not only involved in learning and decision-making processes (27)
111 but also hotspots of various brain disorders (7, 24–26, 28). We identified specific genetic
112 influences on their shapes, investigated genetic asymmetries and similarities among structures,
113 obtained precise estimates of the heritability of these shapes, and performed genetic correlation
114 and enrichment analyses with respect to biological pathways, traits, and diseases.
115

116 Results

118 Multivariate Genome-wide Analyses

119 MOSTest on the LBS of each of the 22 brain structures in 19,862 healthy, unrelated,
120 White-British individuals (10,427 female, with mean age \pm SD of 64.3 ± 7.4 years) yielded a total
121 of 148 significant SNPs (Bonferroni-corrected for multiple testing $p < 1/22 * 5E-8 = 2.27E-9$)
122 which were each independent (linkage disequilibrium (LD) of $r^2 < 0.6$) in their respective LBS
123 GWAS. Some of them were significant in multiple brain structures. Thus, across all 22 GWASs,
124 there were 80 unique SNPs independently associated with the shape of at least one brain structure
125 (Table S1, Fig. S1-S3). Using FUMA (29) for clumping the results of each brain structure (see
126 Methods), we identified 62 genomic risk loci in total, of which 48 were shared by at least 2 of the
127 22 brain structures (Fig. 1). The largest number of independent significant SNPs were found for
128 brain stem (37) (Fig. 2B), followed by left cerebellum white matter (29). Only the amygdala did
129 not show any significant signals after Bonferroni correction. The strongest signal was observed
130 for lead SNP rs13107325 on chromosome 4 with a p-value of 2.15E-74 in association with the
131 LBS of the left cerebellum white matter. This SNP association was observed most frequently,
132 appearing in 14 of the 22 brain structures.

133 49 of the 80 independent SNPs, either themselves or via a proxy variant ($r^2 \geq 0.6$), have
134 previously been identified in GWASs on brain shape-related traits (e.g., volume, surface area, or
135 cortical thickness) and are listed in the GWAS catalog implemented in FUMA. Of these 80, 13
136 have been associated exclusively with other traits (not brain shape-related), and 18 were not
137 related to any GWAS catalog entry (Table S1).

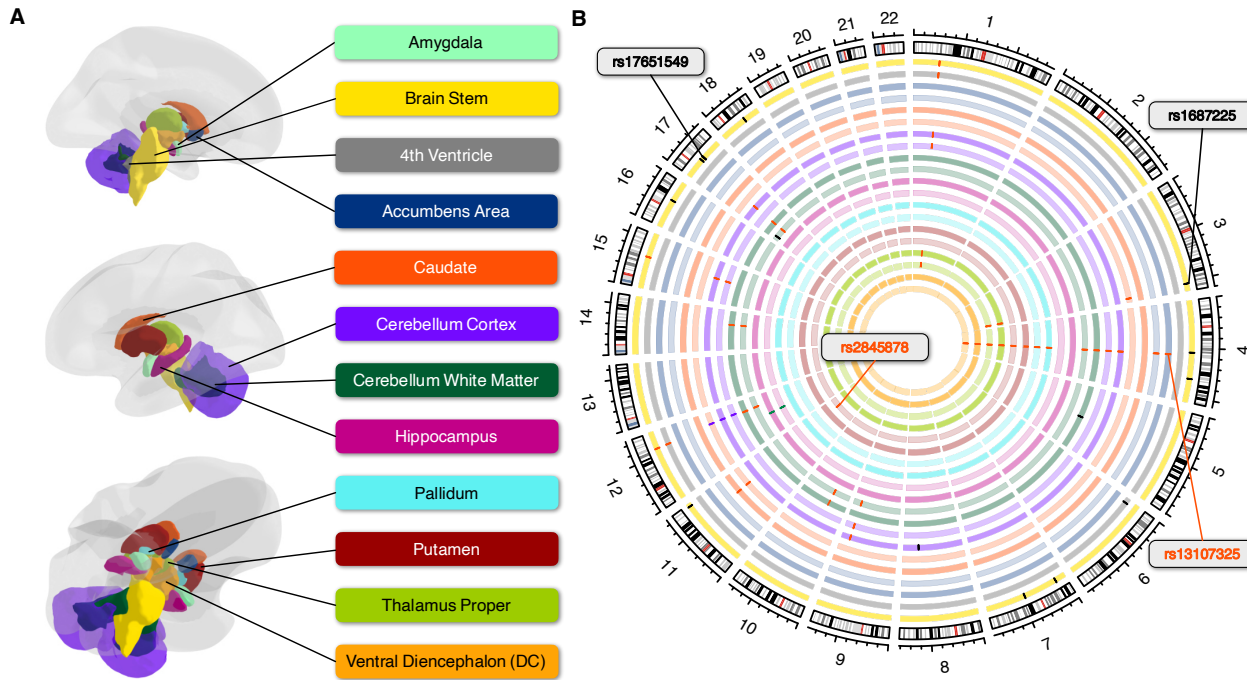


Fig. 1. Overview of Genomic Risk Loci in Different Brain Structures. **A:** Anatomical representation of the subcortical brain structures assessed in the present study. **B:** Circular plot indicating the genomic risk loci derived by MOSTest GWAS on each brain structure. Bilateral structures are on neighboring circles and are the same color as in A, with the right-side structure represented more centrally and lighter. If multiple structures share a locus, the bars indicating their position on the respective circles are the same color.

140 141 Functional Annotations of Genomic Risk Loci

142 We annotated our results using ANNOVAR (30) as implemented in FUMA. Of the 80
143 independent significant SNPs, 3 were exonic, 27 were intronic, and 33 were in intergenic regions
144 (Fig. 2A, Table S2). All 3 exonic variants (rs13107325, rs1687225, rs601558) were
145 nonsynonymous, each having a combined annotation-dependent depletion (CADD) score higher
146 than 15.23 and belong, therefore, to the 3% most deleterious SNPs (31). We further found 28
147 exonic nonsynonymous (ExNS) variants in LD ($r^2 \geq 0.6$) with one of the independent significant
148 SNPs, with 17 of them having a CADD score higher than 15.23 or a Regulome DB score (RDB;
149 small scores indicating a high likelihood of being a regulatory SNP) lower than 2 (Table 1, Table
150 S3).

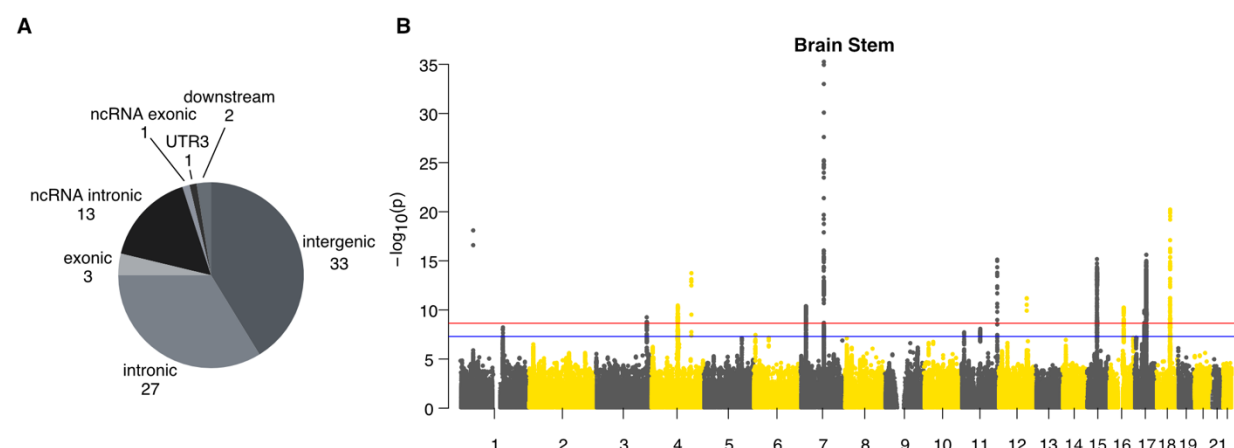


Fig. 2. SNP-based Associations with the LBS. **A:** Pie chart showing the frequency of functional annotations of all 80 independent significant SNPs. **B:** Manhattan plot of multivariate MOSTest results of the brain stem with corrected and non-corrected genome-wide significant threshold ($p=2.27E-9$ (red line), $p = 5E-8$ (blue line)).

151 The pleiotropic missense variant rs13107325, as mentioned above, affects the metal
152 transporter *SLC39A8* and is, with a CADD score higher than 20 (23.1), among the 1% most
153 deleterious SNPs. While ClinVar (32) and AlphaMissense (33) classify this pleiotropic variant as
154 benign, it is a well-known risk factor for schizophrenia (34–36) and has also been found in
155 conjunction with inflammation-based diseases like Crohn's disease (37), blood pressure (38) as
156 well as brain imaging phenotypes (9).

157 *VWA5B2* on chromosome 3 comprises the ExNS missense variant rs1687225, an
158 independent significant SNP associated with brain stem LBS ($p=5.6\text{E-}10$). The CADD score of
159 this variant is relatively high (19), but this SNP is not reported in ClinVar and AlphaMissense
160 predicts it to be likely benign. Of note, the variant is a brain expression quantitative trait locus
161 (eQTL) for different genes and an independent brain cis-eQTL for *VWA5B2* itself according to
162 GTEx (v.8) (Table S4).

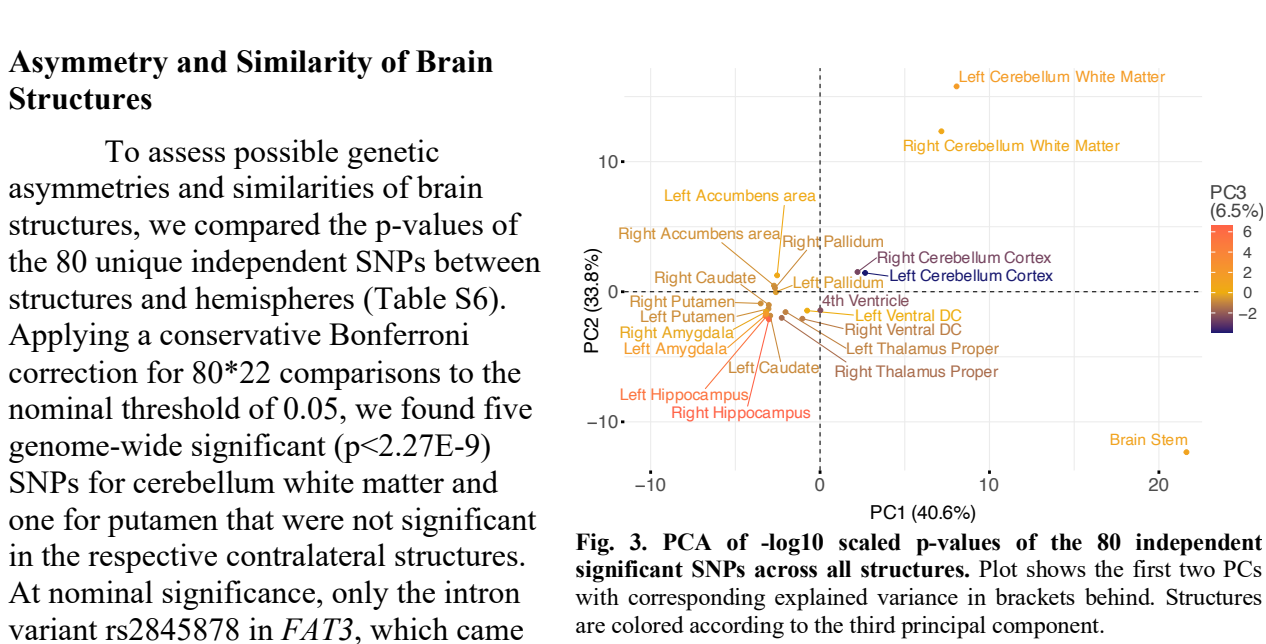
163 The ExNS missense variant rs601558 on chromosome 8 was significantly associated with
164 the LBS of the left cerebellum cortex ($p=8.0\text{E-}11$) and is contained in *RSPO2*, for which it is also
165 a brain eQTL. Despite a high CADD score of 22, this variant is classified as benign by ClinVar
166 and AlphaMissense.

167 Despite its benign classification by ClinVar and AlphaMissense, rs17651549 in *MAPT* on
168 chromosome 17, which was associated with the brain stem LBS at $p=1.0\text{E-}13$, had the highest
169 CADD score (26.8) among the ExNS variants. It was in nearly complete LD ($r^2=0.96$) with the
170 lead SNP rs568589031 (brain stem, $p=2.4\text{E-}16$) of this large genomic risk locus that included
171 altogether 6 ExNS SNPs which, according to CADD score, all belong to the 3% most deleterious
172 SNPs (Table 1) and act as brain eQTLs of *CRHRI*, *SPPL2C*, *MAPT* and *KANSL1*. Due to its high
173 linkage, this large genomic region, also referred to as *MAPT* locus, is known to be highly complex
174 (39) and we observed 18 ExNS SNPs being brain eQTLs of 17 protein-coding genes in total
175 (Table S5).

rsID	Position	EA	NEA	EAF	MinP	CADD	RDB	Gene	Brain Structure (IndSigSNP, r^2)
rs1687225	chr3:183948663	A	G	0.23	6E-10	19.0	4	VWA5B2	Brain Stem (rs1687225 , 1.00)
rs902417	chr3:183951431	T	C	0.25	7E-08	15.4	5	VWA5B2	Brain Stem (rs1687225 , 0.86)
rs3733197	chr4:102839287	A	G	0.35	2E-06	14.2	7	BANK1	Left Cerebellum White Matter (rs114614648 , 0.72)
rs13107325	chr4:103188709	T	C	0.08	2E-74	23.1	5	SLC39A8	Accumbens area (right + left: rs13107325 , 1.00); Cerebellum Cortex (right + left: rs13107325 , 1.00); Cerebellum White Matter (right + left: rs13107325 , 1.00); Pallidum (right + left: rs13107325 , 1.00); Putamen (right + left: rs13107325 , 1.00); Ventral DC (right + left: rs13107325 , 1.00); Thalamus Proper (right: rs13107325 , 1.00; left: rs13135092 , 0.93)
rs7800072	chr7:84628989	G	T	0.32	3E-08	18.3	5	SEMA3D	Brain Stem (rs10247311 , 0.90)
rs601558	chr8:108970367	G	A	0.34	8E-11	22.0	5	RSPO2	Left Cerebellum Cortex (rs601558 , 1.00)
rs36045050	chr14:69257858	T	C	0.26	8E-09	7.0	2b	ZFP36L1	Cerebellum White Matter (right: rs1547050 , 0.74; left: rs12435718 , 0.73)

rs4646626	chr15:58256127	T	C	0.46	6E-15	19.7	NA	ALDH1A2	Brain Stem (rs1061278 , 0.91); Cerebellum Cortex (right: rs3742960 , 0.92; left: rs3742959 , 0.92)
rs1877031	chr17:37814080	A	G	0.33	1E-06	23.1	NA	STARD3	Brain Stem (rs2271308 , 0.80)
rs1058808	chr17:37884037	G	C	0.33	1E-07	23.5	5	ERBB2	Brain Stem (rs2271308 , 0.64)
rs12949256	chr17:43507297	T	C	0.19	1E-08	15.0	4	ARHGAP27	Brain Stem (rs568589031 , 0.70)
rs16940674	chr17:43910507	T	C	0.24	1E-13	17.6	1f	CRHR1	Brain Stem (rs568589031 , 0.96)
rs16940681	chr17:43912159	C	G	0.24	1E-13	5.0	4	CRHR1	Brain Stem (rs568589031 , 0.96)
rs62621252	chr17:43922942	C	T	0.24	6E-14	6.3	5	SPPL2C	Brain Stem (rs568589031 , 0.96)
rs62054815	chr17:43923266	A	G	0.24	1E-13	0.0	5	SPPL2C	Brain Stem (rs568589031 , 0.96)
rs12185233	chr17:43923654	C	G	0.24	5E-14	23.5	1f	SPPL2C	Brain Stem (rs568589031 , 0.95)
rs12185268	chr17:43923683	G	A	0.24	1E-13	8.7	1f	SPPL2C	Brain Stem (rs568589031 , 0.96)
rs12373123	chr17:43924073	C	T	0.24	1E-13	23.3	1f	SPPL2C	Brain Stem (rs568589031 , 0.96)
rs12373139	chr17:43924130	A	G	0.24	1E-13	4.0	1f	SPPL2C	Brain Stem (rs568589031 , 0.96)
rs12373142	chr17:43924200	G	C	0.24	7E-13	7.5	1f	SPPL2C	Brain Stem (rs568589031 , 0.96)
rs63750417	chr17:44060775	T	C	0.24	1E-13	11.9	5	MAPT	Brain Stem (rs568589031 , 0.96)
rs62063786	chr17:44061023	A	G	0.24	9E-14	7.9	5	MAPT	Brain Stem (rs568589031 , 0.96)
rs62063787	chr17:44061036	C	T	0.24	1E-13	0.2	5	MAPT	Brain Stem (rs568589031 , 0.96)
rs17651549	chr17:44061278	T	C	0.24	1E-13	26.8	1f	MAPT	Brain Stem (rs568589031 , 0.96)
rs10445337	chr17:44067400	C	T	0.24	2E-13	19.2	1f	MAPT	Brain Stem (rs568589031 , 0.96)
rs62063857	chr17:44076665	G	A	0.24	1E-13	1.5	7	STH	Brain Stem (rs568589031 , 0.96)
rs34579536	chr17:44108906	G	A	0.24	2E-13	14.4	3a	KANSL1	Brain Stem (rs568589031 , 0.96)
rs34043286	chr17:44117119	G	A	0.24	1E-13	21.0	4	KANSL1	Brain Stem (rs568589031 , 0.96)

Table 1. Exonic Nonsynonymous Variants in LD ($r^2 \geq 0.6$) with one of the Independent Significant SNPs Across all Brain Structures. Variants are listed with non-effect allele (NEA), effect allele (EA), and effect allele frequency (EAF), minimal significance level (minP) across all structures, CADD and RDB scores, most likely affected gene, and the independent significant SNPs (IndSigSNP) to which they are linked most strongly as indicated by the correlation value r^2 . The respective IndSigSNP may differ between brain structures according to the structure-specific GWAS results. Blue-marked variants have CADD > 15.23 or RDB < 2. Bold typing of a variant indicates genome-wide significance in at least one brain structure. Variants in italics are independent significant SNPs.



177
178 **Asymmetry and Similarity of Brain**
179 **Structures**
180 To assess possible genetic
181 asymmetries and similarities of brain
182 structures, we compared the p-values of
183 the 80 unique independent SNPs between
184 structures and hemispheres (Table S6).
185 Applying a conservative Bonferroni
186 correction for $80 * 22$ comparisons to the
187 nominal threshold of 0.05, we found five
188 genome-wide significant ($p < 2.27E-9$)
189 SNPs for cerebellum white matter and
190 one for putamen that were not significant
191 in the respective contralateral structures.
192 At nominal significance, only the intron
193 variant rs2845878 in *FAT3*, which came

194 up in the GWAS on right putamen, lacked symmetry. Proxy variants of rs2845878 ($r^2 \geq 0.6$)
195 have been linked to the mean volume of caudate and putamen according to GWAS catalog (4).
196 Principal component (PC) analysis of -log10 transformed p-values of these 80 SNPs showed a
197 high level of symmetry and similarity in genetic signals (Fig. 3): All subcortical structures as well
198 as the cerebellum cortex were mapped close to each other in this PC space, independent of their
199 hemispherical assignment. Moreover, most structures shared genetic architecture according to
200 their placement adjacent to each other as in case of the basal ganglia, for instance. However, brain
201 stem, cerebellum white matter and hippocampus were substantially distanced from the others in at
202 least one of the first three PCs. Hippocampus was probably notable for its dissimilar pattern of
203 few associated SNPs while the particular position of brain stem and cerebellum white matter
204 could be due to their highly significant signals in addition to their quantity.

205 When investigating genetics that were similar for several structures, the ExNS variant
206 rs13107325 in *SLC39A8* along with several others within the same risk locus on chromosome 4,
207 the intergenic SNP rs6658111 on chromosome 1 and the intronic variant rs12146713 in *NUAK1*
208 on chromosome 12 emerged as the most frequently shared independent SNPs. After Bonferroni
209 correction for 80*22 comparisons, these three were significant in 10 to 15 structures and
210 nominally significant in 19, respectively, 20 structures (Table S6). Apart from the pleiotropic
211 rs13107325, the other two variants have so far only been linked to various brain shape traits such
212 as volume, surface area and cortical thickness according to the GWAS catalog (Table S7).
213 Interestingly, rs12146713 and rs13107325 have also recently been linked to structural
214 connectivity measures (40) which supports the notion that they have an overarching effect on
215 brain structuring.

216 217 Gene-mapping and Gene-enrichment Analysis

218 We first annotated all SNPs passing QC to 18383 protein-coding genes using MAGMA
219 (41) and calculated a p-value for each gene by applying the SNP-wise mean model (see Methods).
220 The brain stem stood out with 20 protein-coding genes being significantly associated with its
221 shape in the gene-based analysis after Bonferroni correction for 22 brain structures and 18383
222 protein-coding genes ($p < 0.05 / (22 * 18383)$) (Fig. 4A). Here, *CRHR1* showed the strongest
223 signal ($p = 5.2E-15$). This gene belongs to the extended *MAPT* locus mentioned above, which
224 came up as generally highly significant and has, together with *MAPT*, which encodes for the
225 microtubule-associated protein tau, often been associated with neurodegenerative disorders (42,
226 43).

227 Next, we used PoPS (44) for gene prioritization, a tool that assigns polygenic priority
228 scores to each gene by fitting their MAGMA z-scores based on trait-relevant gene features
229 extracted from cell-type-specific gene expressions, biological pathways, and protein-protein
230 interactions. Since PoPS works best when combined with orthogonal methods, we also mapped
231 each SNP to the nearest genes. Reranking the genes according to the mean of the two ranks that
232 resulted from the two methods, we prioritized all genes with rank ≤ 2 at each locus (see Methods,
233 Table S8).

234 Based on these genes, a gene set enrichment analysis was conducted using FUMA's
235 Gene2Func method. For bilateral brain structures the two gene sets were joined in this analysis
236 due to similar genetic architectures on both sides (see above and Fig. 3). Afterwards, the overlap
237 and degree of overrepresentation of all prioritized genes in predefined gene sets were examined.

238 At the locus of the most significant SNP in this study, rs13107325, two genes were usually
239 prioritized, *BANK1* and *SLC39A8* (Table S8). The previously known pleiotropy of this genomic
240 region was confirmed by the diversity of our enrichment results which included adventurousness,
241 hypertension, multisite chronic pain, general cognitive ability, and alcohol consumption (Fig. 5A,

242 Fig. S4-S5 for all other structures). Especially the overlap with alcohol consumption was most
243 prominent.

244 These two genes and 23 others were prioritized for the cerebellum white matter. However,
245 given this entire set of genes, *BANK1* and *SLC39A8* were not significantly overrepresented in any
246 gene set. Instead, the other genes, which were primarily prioritized by the cerebellar white matter,
247 were enriched in several regulatory pathways associated with neurological and developmental
248 processes (Fig. 5B).

249 For brain stem, Gene2Func identified gene sets linked to brain morphology and lung
250 function according to GWAS catalog (Fig. 5C) as well as multiple biological processes from the

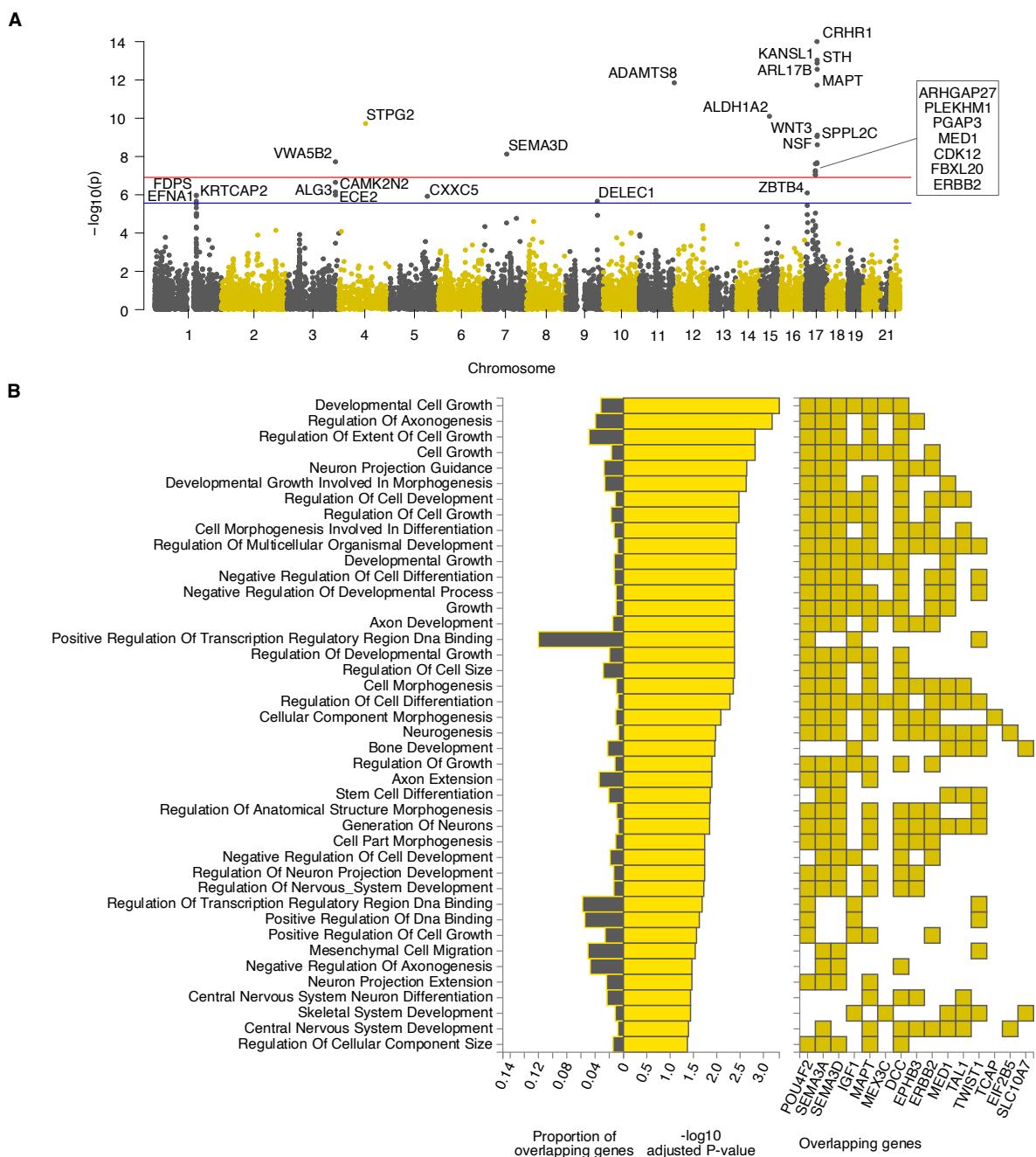


Fig. 4. Gene Analysis and Enrichment in Brain Stem. A: Manhattan plot of MAGMA gene analysis of brain stem results using SNP-wise mean model. **B:** Hypergeometric tests of overrepresentation and overlap of prioritized genes with predefined gene sets using FUMA Gene2Func. Overlap with gene sets of GO biological processes (MsigDB c5). P-values were corrected by the Benjamini-Hochberg method for multiple testing.

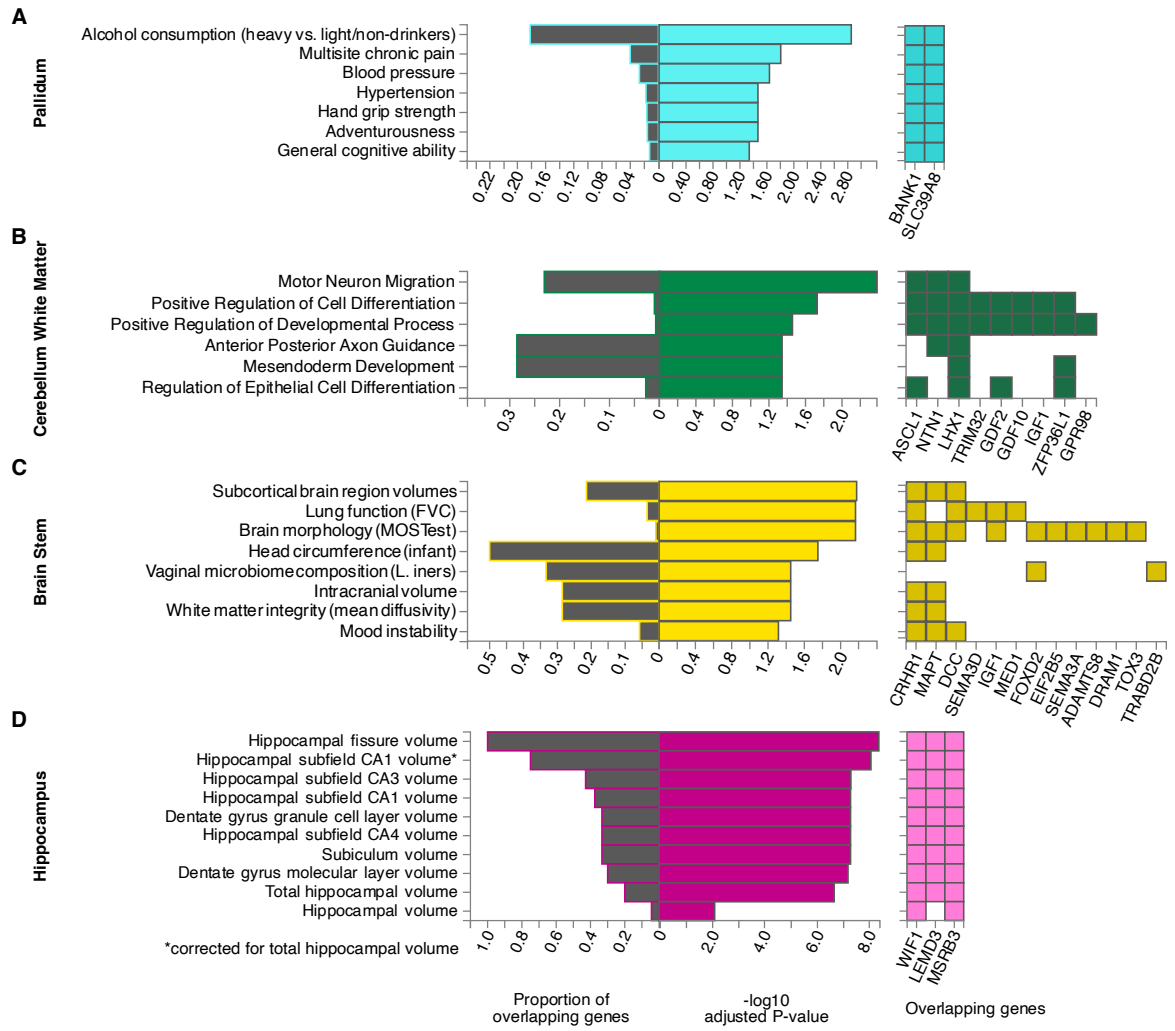


Fig. 5. Significant Gene Enrichment Results of Selected Brain Structures. Hypergeometric tests of overrepresentation and overlap of prioritized genes with predefined gene sets from GWAS catalog traits (A, C, D) and GO biological processes (B). Pallidum (A) was chosen as a representative for structures prioritizing *BANK1* and *SLC39A8* at the pleiotropic locus of rs13107325. All other structures can be found in the supplements. Cerebellum white matter (B), hippocampus (C) and brain stem (D) showed a substantially different genetic pattern before (Fig. 3). P-values were corrected by the Benjamini-Hochberg method for multiple tests in each category.

Gene Ontology Resource (GO) involved in cell and nervous system development and regulation (Fig. 4B). Brain-stem-shape-related genes were additionally enriched in a set of genes differentially expressed in early infancy brain tissue (Fig. S6).

Genes prioritized for hippocampus shape revealed a complete overlap with genes associated with its fissure, but only a partial overlap with its total volume (< 20%), reinforcing the validity and utility of our shape analysis (Fig. 5D).

Associations with Polygenic Risk Scores

To investigate associations between brain-related traits and the LBS of individual brain structures, we extracted polygenic risk scores (PRS) from UKB for Alzheimer's disease (AD), bipolar disorder (BD), ischemic stroke (ISS), multiple sclerosis (MS), Parkinson's disease (PD), and schizophrenia (SCZ). Due to results of our gene-set enrichment analyses (see above), we also included the PRS for alcohol use disorder (ALC) as available in the PGScatalog. 10 of the pairwise partial correlations (i.e. adjusted for covariates, see Methods) between the PRSSs were significant (Bonferroni-corrected $p < 0.05$), most prominently between SCZ and BD ($r = 0.37$,

266 p<1E-300), ALC and SCZ ($r = 0.12$, $p = 1.5\text{E-}60$), and ALC and BD ($r = 0.09$, $p = 1.7\text{E-}38$)
267 (Table S9-S11).

268 Following Sha et. al (45), we performed canonical correlation analysis (CCA) between the
269 LBS of each of the 22 brain structures and each of those PRSs (see Methods). Here, the CCA
270 determined a linear combination of the eigenvalues of an LBS (i.e. the canonical variable) which
271 correlates maximally with the PRS across all examined individuals. We found 31 significant
272 correlations after Benjamini-Hochberg (46) correction ($p < 0.05$) within each PRS, 11 of which
273 also stayed significant after additional Bonferroni correction for 6 independent PRSs (two-level
274 correction), and 6 survived an overall Bonferroni correction for 22*6 tests (Fig. 6). As a balance
275 between false discoveries and sensitivity, we chose this two-level correction to further investigate
276 associations between PRSs and brain structures. Significant correlations ranged from 0.065 to
277 0.080 (mean 0.070). While we found several highly significant correlations with various brain
278 structures for ISS and SCZ, the polygenetic risk for BD and PD did not correlate with any brain
279 shape at all. This is particularly notable since the PRS of BD and SCZ had substantial correlation
280 (see above). The PRSs of AD, ALC, and MS indicated only suggestive correlations with LBSs.

281 To interpret these findings at the level of the eigenvalues, we calculated the mean loadings
282 in each CCA and counted the number of negative and positive values. We noticed that in some
283 results it was possible to assess a common direction of effects. Among all significant results, the
284 right ventral diencephalon (DC) revealed the strongest (i.e. largest absolute) mean loading of -
285 0.295 with 96% of all eigenvalues having a negative correlation with the canonical variable and,
286 in case of a common direction, by that with the PRS of SCZ. This finding suggested that a person
287 may have a higher genetic risk for schizophrenia if the right ventral DC is shaped in such a way
288 that its eigenvalues (frequencies) are lower. This, for example, can be the case for a smoother
289 surface or a less curved shape. A similar deduction in case of brain stem suggested that a less

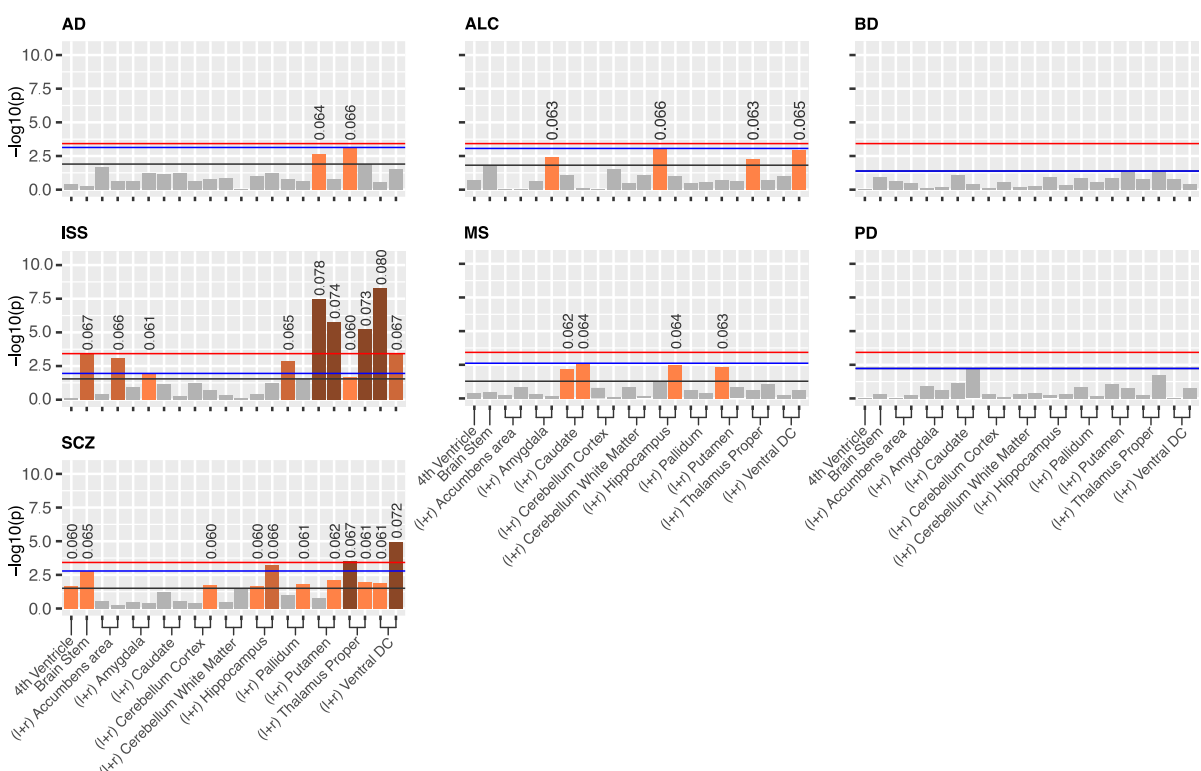


Fig. 6. P-values of CCA Results of Different PRS with Various Brain Structures. Bar charts show the $-\log_{10}$ scaled p-values of the correlations between polygenic risk scores and LBS of different brain structures at different significance levels: Bonferroni-corrected for 22 brain structures and 6 independent PRS (red line), FDR-corrected within each PRS (black line), FDR-corrected within each PRS + Bonferroni-corrected for 6 independent PRS (blue line). Above significant p-values, the correlation value is stated. Bilateral structures are labeled once and the one in the left hemisphere is placed more left.

290 smooth or more curved shape shows a higher risk for ISS (mean loading 0.186 with ~92%
291 loadings positive).

292 Although most correlations remained above the significance threshold, clustering of the
293 mean loadings showed similar tendencies for both hemispheres suggesting no asymmetric
294 behavior (Fig. S7).

295
296 **Heritability**

297 We used SCORE (47) to estimate the univariate heritability of each eigenvalue which
298 utilizes the individual genotype data similar to the analysis by Ge et al. (6). We also calculated the
299 multidimensional heritability (6) (see Methods) for each brain structure (Table 2, Table S12).
300 Overall, the multidimensional heritability of the LBS was significant for all examined brain
301 structures (Bonferroni corrected for 22 structures; range h^2 : [9.5%, 29.6%], mean 17.2%). The
302 highest heritability was found for the caudate (left: 29.6% and right: 27.3%) as well as for the
303 brain stem (28.2%). We further computed the multidimensional LBS heritability for combined
304 structures to compare them with the results from Ge et al. (Table 2, Fig. S8) and found a positive
305 linear correlation (Pearson's $r = 0.735$, $p = 0.038$). However, Spearman's rho did not reach
306 statistical significance ($\rho = 0.714$, $p = 0.058$), suggesting a nonmonotonic relationship.
307 Excluding the 4th Ventricle, which may be an outlier in Ge et al. due to its large standard error and

Brain Structure	h^2	SE	h^2 combined	SE combined	h^2 Ge2016	SE Ge2016
4th Ventricle	0.169	3.0E-3	0.169	3.0E-03	0.005	0.208
Left Accumbens area	0.134	2.8E-3	0.116	1.9E-3	0.237	0.135
Right Accumbens area	0.095	2.4E-3				
Left Amygdala	0.105	2.5E-3	0.118	1.8E-3	-	-
Right Amygdala	0.134	2.8E-3				
Left Caudate	0.296	1.9E-3	0.285	1.4E-3	0.499	0.188
Right Caudate	0.273	2.0E-3				
Brain Stem	0.282	5.4E-3	0.198	1.5E-3	0.452	0.192
Left Cerebellum Cortex	0.186	2.9E-3				
Right Cerebellum Cortex	0.194	2.8E-3				
Left Cerebellum White Matter	0.195	2.6E-3				
Right Cerebellum White Matter	0.148	2.6E-3	0.199	1.9E-3	0.347	0.169
Left Hippocampus	0.187	2.6E-3				
Right Hippocampus	0.210	2.7E-3	0.122	2.0E-3	0.061	0.117
Left Pallidum	0.124	2.9E-3				
Right Pallidum	0.120	2.8E-3	0.183	1.9E-3	0.413	0.148
Left Putamen	0.158	2.7E-3				
Right Putamen	0.210	2.8E-3	0.132	1.9E-3	0.086	0.143
Left Thalamus Proper	0.134	2.7E-3				
Right Thalamus Proper	0.130	2.7E-3	0.146	2.1E-3	-	-
Left Ventral DC	0.122	2.7E-3				
Right Ventral DC	0.169	3.2E-3				

Table 2. Heritability Estimates of Different Brain Structures. Heritability estimates are presented for single brain structures (h^2) and for combined regions (h^2 combined) as well as their standard errors (SE and SE combined). Here, numbers in bold are significant after Bonferroni correction for 22 brain structures. For comparison, the estimates from Ge et al. are listed in the last two columns. Italic numbers are nominally significant and bold ones are significant after false discovery rate correction in (6).

308 very low heritability, both results affirm a significant correlation ($r = 0.844$, $p = 0.017$ and $\rho =$
309 0.786 , $p = 0.048$). We further conducted a Wald test for different heritability in each combined
310 brain structure with $H_0: h^2 = h_{Ge}^2$, which could not be rejected at a 0.05 significance threshold for
311 any of the structures (see Methods and Table S13), implying that our heritability estimates do not
312 differ significantly from those of Ge et al.
313

314 Replication

315 On the 20% replication sample ($N=4961$), we performed a replication analysis of the 80
316 independent SNPs (see Methods). For each brain structure, we only investigated those variants of
317 the 80 SNPs which had also shown Bonferroni-corrected genome-wide significance in the
318 respective discovery GWAS. We replicated 51.4% (76/148) of all significant associations of these
319 80 SNPs at a 0.05 significance level after FDR correction and 60.8% (90/148) at nominal
320 significance level (Table S14). Hence, using a similar replication sample size, our replication rate
321 was at least 33% larger than in van der Meer et al. (2) who introduced MOSTest in their study on
322 brain volumes. To assess what can be expected as replication rate, we split our discovery set into
323 4 sets that equaled the replication set in size and sex and age distribution and checked the
324 “replication rate” in these sets. We obtained rates between 66.2% and 80.4% at FDR-controlled
325 significance and between 68.2% and 82.4% at nominal significance (Table S15). In view of the
326 fact that replication rates of GWASs usually are much lower than expected by power analysis
327 (48% observed vs 91% expected), even after correction for winners’ curse (48% vs 54%) (48),
328 this simple simulation showed that our actual replication rate in a set of independent individuals
329 was in keeping with the size of that set.
330
331

332 Discussion

333 Examining the complex relationship among brain morphology, genetics and neurological
334 disorders is crucial for unravelling the underlying causes and enhancing our understanding of the
335 anatomy of the human brain and diseases. The Laplace-Beltrami operator provides a useful
336 spectral representation for describing shape characteristics. Adequately describing curvatures and
337 being an informative topological fingerprint of the shape (19), the Laplace-Beltrami spectrum
338 (LBS) captures more information compared to global shape quantities such as surface area or
339 volume. Specifically, it captures local shape effects but still represents the whole form of an
340 object since the respective eigenmodes are defined everywhere on the structure. Furthermore, the
341 shape is described by a relatively small number of values, which simplifies data handling, and, in
342 contrast to other dimension reduction methods like principal component analysis, spatial
343 interpretability is still given. Also, it does not depend on error-prone interindividual image
344 registration which is required by other methods. Using the LBS thus allowed us to specifically
345 address the variation in shape independent of volume or surface area and to disentangle the
346 genetics of morphology beyond those global properties. While the eigenmodes and their potential
347 to explain shape-associated biological mechanisms have been recently explored (23), the
348 eigenvalues were previously found to have considerable heritability in the case of subcortical
349 brain structures and cerebellum (6). However, neither the genetic architecture at SNP level of the
350 shape of brain structures nor possible relations to disease genetics have been investigated yet.
351 Using state-of-the-art GWAS and the LBS (a set of eigenvalues) as a multidimensional
352 phenotype, we have dissected the genetics of the shape of 22 brain structures in 19,862 White-
353 British individuals from the UK Biobank.

354 Overall, we identified 148 significant SNP associations that were independent in their
355 respective GWAS. Since some SNPs were significantly associated with more than one brain

356 structure, this resulted in 80 unique significant SNPs being independent across the 22 GWASs.
357 Most of them, particularly the most significant ones, were detected in association with structures
358 in the posterior fossa (brain stem and cerebellum). In contrast, we found no significant signal for
359 the LBS of the amygdala. Due to the simple almond-like shape, crude measures like volume and
360 surface area might already capture amygdala's shape well enough (Supplements, Table S16). This
361 could possibly explain the lack of genetic signal in our study since we controlled for both volume
362 and surface area.

363 Of those 80 SNPs, 37 have previously been reported as genome-wide significant in a large
364 GWAS on subcortical volumes (2), while 4 were identified in a large GWAS meta-analysis on
365 total brain volume (1). This overlap with volume-associated SNPs suggests pleiotropic effects of
366 the respective gene loci, affecting both volume and shape characteristics independent of volume,
367 while it is unlikely that pure volume associations were picked since we controlled for volume.
368 Indeed, our hippocampus LBS GWAS, for instance, replicated 100% of all loci previously
369 associated with hippocampal fissure size (49), which obviously influences hippocampal shape,
370 while accounting for only 20% of the loci associated with total hippocampal volume (Fig. 5D).

371 31 of the 80 independent SNPs were not associated with any brain shape-related trait
372 according to GWAS catalog, neither by themselves nor by any variant in LD with them ($r^2 \geq$
373 0.6), and 18 were not listed at all (Table S1). This shows a substantial degree of novelty, that is,
374 undiscovered genetic effects specific to shape of brain structures and supports the notion of SNPs
375 affecting the development of form independent of growth.

376 Using a 15 times larger sample size, we were able to substantially refine the LBS SNP-
377 heritability estimates of subcortical brain structures, including cerebellum, previously provided by
378 Ge et al. (6) (N=1320). While their estimates ranged from 0.005 to 0.5, some being non-
379 significant due to large standard errors of 0.12 to 0.21, our estimates were between 0.1 and 0.3, all
380 being significant with much lower standard errors (≤ 0.005). In fact, statistical tests implied that
381 our heritability estimates did not differ significantly from those of Ge et al. This was likely due to
382 the much larger standard errors of their estimates but may also be a consequence of the younger
383 age span in their cohort (18-35 years). Overall, we achieved results with higher statistical
384 significance corresponding to our larger sample size and also likely due to our additional control
385 for total brain volume, the respective local surface area, and MRI scan quality. The refined
386 estimates were approximately equal to the SNP-heritability of volumetric traits of subcortical
387 structures which Hibar et al. (3) derived from similar sample sizes, or even larger as in the case of
388 caudate, hippocampus and putamen, for which they derived a SNP-heritability of about 0.11 with
389 95%-CI < 0.16 each, while we found values of 0.29, 0.20, and 0.18 respectively.

390 Bilateral structures showed similar genetic architecture of LBS (Fig. 3), which could be
391 expected due to their symmetry. Moreover, genetic architecture was also shared between
392 structures, as suggested by their adjacent positions, e.g. in the case of the basal ganglia. The two
393 noticeably frequently shared variants rs13107325 and rs12146713 on *SLC39A8* and *NUAK1*,
394 respectively, seem to affect brain shape globally as they have recently been associated with the
395 structural connectome (40). While *SLC39A8*, as a brain metal transporter, is involved in several
396 brain and neurodevelopmental traits (see below), *NUAK1* is also known to regulate axon
397 branching by controlling mitochondrial distribution (50). The genetic associations of cerebellum
398 and brain stem LBS were more different. Brain stem stood out due to a high number of specific
399 association signals. These included the exonic nonsynonymous (ExNS) variant rs1687225 in
400 *VWA5B2*, the gene of von Willebrand factor A domain containing protein 5B2. This missense
401 variant belongs to the 3% most deleterious variants (according to CADD score) and was also an
402 independent brain cis-eQTL of *VWA5B2* according to GTEx (v.8). Proxy variants of rs1687225

403 have been reported as being associated with brain morphology (2), cortical thickness (51), and
404 educational achievement (52).

405 An extended genomic risk locus on chromosome 17 with lead SNP rs568589031 was also
406 rather specific for the brain stem. ExNS variant rs17651549 at this locus had the highest CADD
407 score (26.8) of all variants in LD with any of the independent significant SNPs. It affects *MAPT*
408 which was among the most significant signals in MAGMA gene-based analysis of the brain stem
409 LBS. However, this locus contains multiple protein-coding genes with several brain cis-eQTLs
410 affecting them and other genes in the region (Table S5). The analysis of this large locus is highly
411 challenging. The locus has previously been mapped to brain morphology (2) and several
412 neurodegenerative diseases such as progressive supranuclear palsy, corticobasal degeneration,
413 frontotemporal dementia, Parkinson's disease, and Alzheimer's disease (AD) (42, 43, 53–62).
414 Moreover, variations in cortical morphology have recently been linked to *APOE* ε4 and *MAPT* in
415 young healthy adults (63). There is also evidence of brain stem deformations in early stages of
416 AD manifesting as variations in the midbrain (64), decreased locus coeruleus (part of the brain
417 stem) volume preceding neuronal loss (65), and neurofibrillary tangle-related neurodegeneration
418 in the brain stem potentially causing neuropsychiatric symptoms (66). While patients with
419 diagnosed neurodegeneration were excluded from our study, the possibility remains that
420 preclinical stages might potentially mediate the genetic relation between shape and the *MAPT*
421 locus. However, neither gene enrichment analysis (Fig. 4 and 5) nor Canonical Correlation
422 Analysis (CCA, Fig. 6), as an enrichment analysis independent of candidate genes, did provide
423 evidence for a significant correlation between the genetics or phenotype of brain stem LBS and
424 the genetics, respectively the PRS, of neurodegeneration such as AD.

425 At this locus, significant ExNS SNPs with high CADD scores were also found in
426 *SPPL2C*, *KANSL1* and *CRHR1*, which showed the strongest signal in the MAGMA analysis
427 (Table 1, Fig. 4A). Loss-of-function variants of *KANSL1* are known for causing autosomal-
428 dominant Koolen-de-Vries syndrome (MIM #610443) which is characterized by intellectual
429 disability and structural brain abnormalities (67). *SPPL2C* is the gene of signal peptide peptidase-
430 like 2C and has previously been highlighted in a GWAS on total brain volume due to a relatively
431 large number of ExNS (1). However, we controlled for volume in our GWAS of brain shape. A
432 recent study found that *CRHR1*, which encodes a receptor for the corticotropin-releasing hormone
433 CRH, moderates brain volume differences, possibly through its stress response function, which in
434 return mediates the relationship between urban environmental exposure and affective symptoms
435 (68). Especially, in the context of *CRHR1*, lower brain volume was observed in relation to
436 stronger affective symptoms and greater urban environment exposure. Variants of *CRHR1*, have
437 further been associated with alcohol (69) and heavy alcohol consumption following stressful life
438 (70). Even light alcohol consumption has recently been related to changes in brain structure (71).
439 Indeed, genes associated with the LBS of several other brain structures were enriched in gene sets
440 associated with alcohol consumption (Fig. 5A, Fig. S4-S5). Thus, alcohol consumption may be a
441 potential mediator of their effect on brain shape. However, we would like to note that the
442 enrichment was driven by one locus.

443 That locus on chromosome 4 with lead SNP rs13107325, an ExNS variant of *SLC39A8*,
444 appeared not only to be significant in most brain structures (15 structures including the brain
445 stem, albeit with subthreshold significance) but also revealed the overall strongest signal across
446 all the GWASs in left cerebellum white matter. This locus, especially the lead SNP, has a
447 pleiotropic effect. Besides alcohol consumption (72), it has been linked to schizophrenia (SCZ)
448 (34–36), Crohn's disease (37), blood pressure and cardiovascular disease risk (38), and several
449 brain imaging phenotypes (9). The cerebellothalamic and cerebellar-basal ganglia connectivity
450 dysfunction hypothesis in individuals with SCZ is supported by the significant and prominent

451 occurrence of rs13107325 in precisely these regions (73, 74). SCZ is known to be associated with
452 abnormalities of subcortical brain structures (75–77). Clinical features of SCZ might be due to
453 aberration of dendritic spine density (78). A knock-in mouse model of rs13107325 points to an
454 increased risk of SCZ by regulating zinc transport and dendritic spine density and subtle effects
455 on cortical development due to this variant (79). A recent gene-mapping study concluded strong
456 evidence for pleiotropic genes associated with SCZ and brain structure with evidence of brain
457 variation causing SCZ (80).

458 SCZ shows substantial genetic correlation (0.68) with bipolar disorder (BD) (81) which
459 was also evident in the correlation (0.37) between their PRSs. However, BD seems to have less
460 relation to brain morphology. Madre et al. (82) investigated cortical morphology in individuals
461 with SCZ and BD and reported shared volume and thickness deficits while abnormalities of
462 geometry and curvature were specific to SCZ. Also, Stauffer et al. reported the association of
463 MRI metrics to be weaker with BD genetics than with SCZ genetics (80). Our results are in line
464 with these findings as CCA revealed correlation of the LBS of several brain structures only with
465 the SCZ-PRS while there was no correlation with BD-PRS (Fig. 6). This result suggests that LBS
466 may therefore be sensitive to SCZ-specific brain shape variations and thus potentially helpful for
467 the differential diagnosis of psychosis.

468 CCA also revealed highly significant links between the LBS of multiple brain structures
469 and the PRS of ischemic stroke (ISS) in our healthy cohort (Fig. 6). In line with the high
470 correlation between ISS-PRS and hypertension (HT) PRS, CCA produced a very similar result for
471 the HT-PRS (Fig. S9). HT is associated with white matter hyperintensities and cognitive
472 dysfunction in elderly patients and is a major risk factor for ISS (83). A recent study showed that
473 morphological changes in the basal ganglia and thalamus already occurring in mid-life are
474 associated with blood pressure and, therefore, might be better markers of early HT than volume
475 aberrations (84). Our CCA results were especially significant in these brain regions, which in turn
476 support the suggestion of using brain morphology or shape as an early biomarker of HT.

477 Limitations of our study include the lack of effect sizes (beta values) in our multivariate
478 results, which impedes the use of conventional post-GWAS tools such as genetic correlation and
479 Mendelian randomization analyses. Instead, we explored the relationship to genetics of other
480 traits by performing CCA between LBSs and PRSs. This was limited by the predictive power of
481 each PRS. Furthermore, we cannot establish causal relationship between genetic variation in brain
482 morphology and a particular trait or disease. Restricting our study to healthy individuals may
483 additionally have yielded lower effect sizes and potentially false negative correlations when
484 performing disease-related analyses. A follow-up of our findings, therefore, provides avenues for
485 future research.

486 In summary, we have provided the first delineation of the genetic architecture of brain
487 shapes beyond global measurements such as volume and surface area by using the Laplace-
488 Beltrami spectrum as a mathematical shape descriptor. In our multivariate GWAS on a large
489 healthy cohort of the UK Biobank, we identified 80 unique independent SNPs with brain stem
490 showing a distinctly high number of specific association signals which included the *MAPT* locus
491 implicated in neurodegenerative diseases. The shapes of most brain structures were significantly
492 associated with the pleiotropic variant rs13107325, a known risk factor for schizophrenia. We
493 further identified significant correlations between brain shape and polygenic risk scores of
494 schizophrenia, hypertension and ischemic stroke, suggesting the potential use of the LBS as an
495 early disease biomarker. As such, the LBS expands the set of tools for investigating brain shapes,
496 holding implications for early detection of a wide spectrum of traits and warrants further research
497 in disease-specific cohorts.

498 **Materials and Methods**

499

500 **UKB Data and Sample Filtering**

501

502 Data was retrieved from the official source of the [UK Biobank](#) (application number 41655) and
503 provided as a DataLad dataset, a research data management solution providing data versioning,
504 data transport, and provenance capture (85). A total of 487,409 genotyped samples were available
505 (v3 imputed on Haplotype Reference Consortium and UK10K haplotype data, aligned to the +
506 strand of the reference and GRCh37 coordinates, released in 2018, data field 22828). We kept
507 only self-reported White-British individuals for data homogeneity according to data field 21000,
508 resulting in 430,560 individuals. After genetic quality control (QC, see below), there were
509 393,913 unrelated samples left. 30,080 of them had structural MRI data (T1) on which we
510 calculated the LBS (see below) of 22 brain structures (Fig. 1) of 24,834 individuals without
511 mental or behavioral disorders (ICD index F) or diseases of the nervous system (ICD index G)
512 according to the International Statistical Classification of Diseases and Related Health Problems
513 10th revision (ICD-10).

514 We created age and sex-stratified discovery and replication samples by splitting the data into 2
515 subsets comprising 80% and 20% of the individuals, respectively. Excluding samples without
516 total brain volume data (see below), our final data set for our discovery GWAS contained 19,862
517 individuals, 9435 male and 10,427 female, ranging in age between 46.0 and 81.7 years with a
518 mean \pm SD of 64.3 \pm 7.4 years (female: 63.6 \pm 7.3, male: 65.0 \pm 7.5).

519

520 **Quality Control of Genetic Data**

521

522 We conducted QC using whenever possible Plink2 (86) and Plink (v1.9) for some missing
523 functionalities on all self-reported White-British individuals and their imputed genotype data,
524 which was initially converted from BGEN to binary Plink2 format, and kept only single-
525 nucleotide polymorphisms (SNPs). As recommended by UK Biobank (87), we removed variants
526 with an imputation score less than 0.3, and following Mills et al. (88), we excluded all variants
527 with a call rate less than 0.95, a minor allele frequency of less than 0.01 and a Hardy-Weinberg
528 equilibrium exact test p-value below 1E-6. As recommended by Plink2, we used the mid-p
529 adjustment to reduce the filter's tendency to retain variants with missing data (89) and the *keep-*
530 *fewhet* modifier. We also removed samples with a mismatch between self-reported and
531 genetically inferred sex, with genotype missingness of more than 0.05, and all heterozygosity
532 outliers (± 3 SD). Moreover, using a kinship coefficient of 0.088 and the *king-cutoff* command,
533 we randomly excluded one from each pair of individuals related to \geq 2nd degree. Only autosomal
534 SNPs were examined. In total 8,105,763 SNPs remained after QC. We calculated the first 10
535 principal components (PC) from them, which were included as covariates in the GWASs.

536

537 **Image Data Processing**

538

539 First, we segmented anatomical structures from all available T1 MRI brain scans with FreeSurfer
540 version 7.2.0 (90–94). Second, we created triangular meshes for all structures of interest. Finally,
541 we computed compact shape representations for all structures, using the BrainPrint Python
542 package (21) (see below). To account for the quality of the MRI scans, we computed the Euler
543 number with FreeSurfer. This represents the total defect index and is a measurement of the
544 number of holes in the calculated surface.

545

546

547 **Multidimensional Shape Descriptor**

548
549 A shape, parametrized as a Riemannian manifold M , may be described by its intrinsic geometric
550 information, which can be obtained by solving the Helmholtz equation on that manifold:

551
552
$$\Delta f = -\lambda f,$$

553

554 where Δ is the Laplace-Beltrami operator, a generalization of the Laplace operator in Euclidean
555 space, and f a real-valued function, with $f \in C^2$, defined on M . The solutions (f_i, λ_i) represent
556 the spatial part of the wave equation with eigenfunctions f_i and eigenvalues λ_i where $\sqrt{\lambda_i}$ can be
557 interpreted as the natural frequencies. The set of all eigenvalues is called the spectrum of an
558 operator. The LBS or Shape-DNA (13) is accordingly defined as the beginning subsequence of
559 the increasingly ordered spectrum of the Laplace-Beltrami operator solved on a Riemannian
560 manifold:

561
562
$$\{\lambda_1, \dots, \lambda_N\} \text{ with } 0 \leq \lambda_i \leq \lambda_j \quad \forall i < j.$$

563

564 The LBS was computed with the BrainPrint package (21) based on the FreeSurfer output. For
565 each individual, we calculated the first, i.e., the smallest, 50 eigenvalues of each brain structure as
566 done in (6). Because the first eigenvalue is always zero, since each object is a closed surface
567 without boundary, we used only the next 49 values in our analyses. Each eigenvalue $\lambda_{i,m}$ was
568 further normalized to volume V_i of each brain structure i . Volume and surface area were
569 calculated by BrainPrint. Afterwards $\lambda_{i,m}$ was divided by its position m in the ordered spectrum
570 to balance out the higher eigenvalues which more likely represent noise (6, 13, 21):
571

$$\bar{\lambda}_{i,m} = \frac{1}{m} (\lambda_{i,m} \cdot V_i^{\frac{2}{3}}), \forall i \in \{1, \dots, 22\}, m \in \{2, \dots, 50\}$$

572
573 In the end, we analyzed 22 brain structures as provided by FreeSurfer: 4th ventricle, brain stem,
574 accumbens area (left and right), amygdala (left and right), caudate (left and right), cerebellum
575 cortex (left and right), cerebellum white matter (left and right), hippocampus (left and right),
576 pallidum (left and right), putamen (left and right), thalamus proper (left and right), ventral
577 diencephalon (DC) (left and right). By that, we handled the normalized and reweighted LBS
578 $\{\bar{\lambda}_{i,2}, \dots, \bar{\lambda}_{i,50}\}$ for each brain structure i as a 49-dimensional quantitative trait.
579

580
581 **Multivariate Genome-wide Association Analysis**

582
583 For our multivariate GWAS, we used the MOSTest tool, a multivariate omnibus test, which
584 handles big data efficiently and accounts for the correlation among the phenotypes to increase
585 statistical power (2). Since the eigenvalues are not independent in general (Pearson correlation
586 range: [0.285;0.998], mean \pm SD 0.93 ± 0.06 , Fig. S10-S12), we conducted, for each brain structure
587 i , a multivariate GWAS on the 49 volume-normalized and scaled eigenvalues $\bar{\lambda}_{i,m}$, $m \in$
588 $\{2, \dots, 50\}$, treating each $\bar{\lambda}_{i,m}$ as a single quantitative phenotype. For that, we first calculated
589 residuals of the multidimensional phenotype to control for potential covariates as recommended
590 by MOSTest, i.e., we regressed each $\bar{\lambda}_{i,m}$ on age, age², sex, first 10 genetic principal components
591 (PCs), Euler number, surface area of each brain structure i and the total brain volume. The latter
592 was calculated as the sum of the volume of ventricular cerebrospinal fluid (data field 25004) and
593 the gray and white matter volume (data field 25010) in line with Jansen et al. (1). Normalizing the
594 LBS to volume as described above and regressing out total brain volume and surface area of each

595 brain structure assured that we indeed studied the shape and not linear size effects. We defined the
596 residualized eigenvalues $\tilde{\lambda}_{i,m}$ as the sum of the estimated intercept and the residuals of its linear
597 regression. After adjusting for covariates, the range of absolute correlations between all $\tilde{\lambda}_{i,m}$ was
598 quite high (Pearson correlation range: [0;0.978], mean \pm SD 0.65 \pm 0.18, Fig. S10-S12). We further
599 inspected the relation of each $\tilde{\lambda}_{i,m}$ to volume and surface area by calculating their Pearson
600 correlations. There was, as expected, no correlation with surface area and a low correlation with
601 volume (average $r = 0.28$) (Fig. S13). The effect was small except for the eigenvalues of caudate,
602 which showed a mean correlation of 0.50 (left) and 0.45 (right), likely relating to the long C-
603 shaped form of that structure and by the fact that volume normalization (i.e. multiplication with
604 $V_i^{\frac{2}{3}}$, see above) excludes the pure size effects but not a real difference in shape. Including volume
605 as additional covariate in the MOSTest analysis produced nevertheless similar results (Table
606 S17).

607 All $\tilde{\lambda}_{i,m}$ were then passed to MOSTest, which first performs a rank-based inverse-normal
608 transformation (INT) to obtain normally distributed data. This is followed by a standard additive
609 univariate GWAS for each $\tilde{\lambda}_{i,m}$, resulting in z-scores for each SNP and $\tilde{\lambda}_{i,m}$. This procedure is
610 repeated with once-permuted genotypes, preserving phenotype correlation. The MOSTest test
611 statistic for a SNP is then calculated as the Mahalanobis norm of the non-permuted z-scores of
612 that SNP and the correlation matrix R of the z-scores from once-permuted genotypes of all
613 eigenvalues. The p-value of the multivariate test statistic is then calculated from a cumulative
614 distribution function of a fitted gamma distribution, which eliminates the need for a multiple
615 testing correction of 49 univariate GWASs and therefore allows to determine significance of
616 SNPs with a p-value below the standard genome-wide threshold of 5E-8. We further confirmed
617 that MOSTest controlled the type-I error sufficiently by plotting p-values from empirical
618 distributions of the test statistic and from fitted gamma functions under the null hypothesis as
619 calculated by permutating the phenotype-genotype assignments (Fig. S14-S35).

620 Identification of Genomic Loci and Functional Annotations

621

622 For functional annotations, we used the web-based platform FUMA (v1.5.6) (29). We used
623 default settings to determine genomic risk loci. First, independent significant SNPs were
624 identified as the ones with p-value equal to or smaller than 2.27E-9 (Bonferroni correction for 22
625 brain structures 5E-8 / 22 = 2.27E-9) and linkage disequilibrium (LD) with other such SNPs in its
626 vicinity of $r^2 < 0.6$. These SNPs and those in LD with them ($r^2 \geq 0.6$) were defined as
627 candidate SNPs and used in subsequent analyses. LD computation was based on the European
628 population within the 1000 genomes reference panel (phase 3) (95). Those with $r^2 < 0.1$ were
629 classified as lead SNPs among the independent significant SNPs. Independent significant SNPs
630 with $r^2 \geq 0.1$, or with a gap of less than 250 kb between their respective LD blocks (all SNPs in
631 LD $r^2 \geq 0.6$ with them) were merged into one genomic risk locus. Therefore, a genomic risk
632 locus can contain multiple independent significant SNPs.

633 Candidate SNPs were used for functional annotations. Positional annotation was performed with
634 ANNOVAR (30). Further, SNPs were annotated with CADD scores, RegulomeDB scores, and
635 15-core chromatin states. The major histocompatibility (MHC) region was excluded from all
636 annotations. For eQTL mapping, we checked several available databases containing relevant
637 information, i.e., PsychENCODE eQTLs, ComminMind Consortium, BRAINEAC, and GTEx v8
638 Brain, and extracted all significant SNP-gene pairs with a False Discovery Rate (FDR, Benjamini-
639 Hochberg procedure(46)) controlled p-value < 0.05 within the respective database.

640
641
642

643 Gene-mapping and Gene-enrichment Analysis

644
645 For gene prioritization, we used PoPS (v 0.2) (44), a tool that assigns polygenic priority scores to
646 each gene by fitting their MAGMA z-scores by trait-relevant gene features extracted from cell-
647 type-specific gene expression, biological pathways and protein-protein interactions. We
648 calculated these z-scores using MAGMA (v 1.10) (41) by first annotating SNPs to 18,383 protein-
649 coding genes within a 0kb window and afterwards performing gene analysis using the SNP-wise
650 mean model and the European population of 1000 Genomes as reference dataset for every brain
651 structure. We then ran PoPS on our MAGMA scores using default settings and all available
652 57,543 gene features. Gene annotation and location files, as well as gene features, were taken
653 from <https://www.finucanelab.org/data>.

654 Lead SNPs, as defined by FUMA (see above), were mapped to genes within a 500kb window up-
655 and downstream. We first selected the four genes with the highest PoP score in each locus.
656 Second, since it was shown that PoPS works best when combined with orthogonal methods like
657 Nearest Gene, we mapped each lead SNP to the two closest genes. After assigning a rank to each
658 gene by both methods and averaging the two ranks, we reranked the genes and finally prioritized
659 all genes with average rank ≤ 2 for each independent significant SNP.

660 The prioritized genes were given as input to FUMAs Gene2Func tool. Genes of brain structures
661 present in both hemispheres were joined in each analysis. We used all protein-coding genes of
662 Ensembl v110. Hypergeometric tests analyzed the overrepresentation of mapped genes in
663 precalculated gene sets followed by an FDR control (Benjamini-Hochberg, $p < 0.05$) within each
664 category.

665 Canonical Correlation Analysis with PRS

666 For the canonical correlation analysis (CCA), we extracted PRS of 6 brain shape-related traits and
667 disorders and of one trait that stood out from the FUMA gene-set results. 6 PRS were taken from
668 the UK Biobank which have exclusively been trained on external data sets: Alzheimer's disease
669 (data field 26206), bipolar disorder (data field 26214), ischemic stroke (data field 26248),
670 multiple sclerosis (data field 26254), Parkinson's disease (data field 26260) and schizophrenia
671 (data field 26275). Further, we calculated the PRS for alcohol use disorder based on the score
672 definition from the PGScatalog (96) (PGS002738 (97)). UK Biobank data was not used for
673 training in this last score but for one GWAS in the discovery meta-analysis of the alcohol use
674 disorder study. The data was available for 19850 samples. Each PRS was first linearly regressed
675 on age, age², sex, first 10 genetic principal components (PCs), and total brain volume. The
676 residuals were added to the fitted intercept. Second, a rank-based INT was applied to those
677 PRS. The partial correlation between the PRS was calculated as a Pearson correlation. We used
678 the residualized eigenvalues $\tilde{\lambda}_{i,m}$ as they were used as input for MOSTest for each brain structure
679 and applied a rank-based INT.

680 For each pair of PRS and brain structure, we conducted a CCA using the cca() function within the
681 "yacca" R-package (version 1.4-2) (98). CCA finds a linear combination of all eigenvalues, a so-
682 called canonical variable, which correlates maximally with the PRS. All resulting p-values of the
683 correlations were adjusted for multiple testing using FDR. Afterwards, we applied an additional
684 Bonferroni correction for 6 effective PRS, which we consider as the two-level correction. For
685 comparison, we also calculated the Bonferroni correction for 22*6 tests. All adjustments were
686 made to the 0.05 significance threshold.

687 Further, in each CCA, we investigated the loadings, i.e. the correlations of all eigenvalues with
688 their canonical variable, which describe the direction and strength of the impact of each
689 eigenvalue on the risk score. Out of those, we calculated the mean loading and the number of
690 negative/positive loadings of all eigenvalues in each brain structure and PRS. If at least 90% of all
691

693 loadings had the same direction, we deemed that as a common direction of effects. Hierarchical
694 clusters were computed on the distances of mean loadings among brain structures and PRS,
695 respectively, using the complete linkage method (Fig. S7).

696

697 SNP-based Heritability

698

699 Ge et al. investigated the heritability of neuroanatomical shape using the LBS. For estimating its
700 SNP-heritability, they proposed a multidimensional approach where they summed the univariate
701 heritability h_m^2 of the eigenvalues, each weighted by γ_m , the relative size of its phenotypic
702 variance:

703

$$704 h^2 = \sum_m \gamma_m h_m^2, \text{ with } \gamma_m = \frac{\sigma_{Pm}^2}{\sum_k \sigma_{Pk}^2},$$

705

706 and σ_{Pm}^2 being the phenotypic variance of trait m . The univariate heritabilities of the 49
707 eigenvalues were derived using SCORE. For combined structures, we derived the
708 multidimensional heritability from the union set of eigenvalues. When applying SCORE, we
709 proceeded as with the GWAS described above, using volume-normalized and reweighted
710 eigenvalues and the same set of covariates. The phenotypic variance was also computed using the
711 residualized eigenvalues $\tilde{\lambda}_{i,m}$. We further calculated the p-value of each heritability using the
712 Wald test statistics, which is distributed as

713

$$714 \left(\frac{h^2}{SE(h^2)} \right)^2 \sim \frac{1}{2} \chi_0^2 + \frac{1}{2} \chi_1^2$$

715

716 With χ_0^2 being the point mass at 0 and χ_1^2 the chi-squared distribution with one degree of freedom
717 since the null hypothesis $H_0: h^2 = 0$ lies on the boundary of a constrained parameter space ($h^2 \geq$
718 0) (99). The standard error (SE) of each multidimensional heritability was calculated using
719 Bienaymé's identity for the variance of a sum and the univariate estimates from SCORE as
720 follows:

721

$$722 SE(h^2) = \sqrt{\sum_m \gamma_m^2 SE(h_m^2)^2}.$$

723

724 For testing the difference between heritability values in each combined brain structure, we
725 utilized the Wald test statistics distributed as

726

$$727 \left(\frac{h^2 - h_{Ge}^2}{SE(h^2 - h_{Ge}^2)} \right)^2 \sim \chi_1^2,$$

728

729 with

730

$$731 SE(h^2 - h_{Ge}^2)^2 = SE(h^2)^2 + SE(h_{Ge}^2)^2 - SE(h^2)SE(h_{Ge}^2)cor(h^2, h_{Ge}^2).$$

732

733 Since $SE(h^2)$ is small in comparison to $SE(h_{Ge}^2)$, we can approximate $SE(h^2 - h_{Ge}^2)^2$ by just
734 $SE(h_{Ge}^2)^2$.

735

736

737

Replication

738

739 Replication analysis was conducted on the 20% sample (see above). This encompassed 4963
740 individuals, of which 4961 (2605 female) had data of total brain volume available, ranging in age
741 from 45.2 to 81.8 years (age mean \pm SD: 64.2 \pm 7.4, female: 63.6 \pm 7.2, male: 64.9 \pm 7.6). We used
742 the same procedure and set of covariates to perform MOSTest analyses for each brain structure on
743 this dataset and all SNPs passing QC. For each brain structure, we only investigated those variants
744 of the 80 independent SNPs which had shown Bonferroni corrected genome-wide significance in
745 the respective discovery GWAS. FDR correction was applied to these p-values for each brain
746 structure separately.

747

748

749

750

References

751

- 752 1. P. R. Jansen, M. Nagel, K. Watanabe, Y. Wei, J. E. Savage, C. A. De Leeuw, M. P. Van Den Heuvel, S. Van
753 Der Sluis, D. Posthuma, Genome-wide meta-analysis of brain volume identifies genomic loci and genes shared with
754 intelligence. *Nat Commun* **11**, 5606 (2020).
- 755 2. D. Van Der Meer, O. Frei, T. Kaufmann, A. A. Shadrin, A. Devor, O. B. Smeland, W. K. Thompson, C. C.
756 Fan, D. Holland, L. T. Westlye, O. A. Andreassen, A. M. Dale, Understanding the genetic determinants of the brain
757 with MOSTest. *Nat Commun* **11**, 3512 (2020).
- 758 3. D. P. Hibar, J. L. Stein, M. E. Renteria, A. Arias-Vasquez, S. Desrivière, N. Jahanshad, R. Toro, K.
759 Wittfeld, L. Abramovic, M. Andersson, B. S. Aribisala, N. J. Armstrong, M. Bernard, M. M. Bohlken, M. P. Boks, J.
760 Bralten, A. A. Brown, M. Mallar Chakravarty, Q. Chen, C. R. K. Ching, G. Cuellar-Partida, A. den Braber, S.
761 Giddaluru, A. L. Goldman, O. Grimm, T. Guadalupe, J. Hass, G. Woldehawariat, A. J. Holmes, M. Hoogman, D.
762 Janowitz, T. Jia, S. Kim, M. Klein, B. Kraemer, P. H. Lee, L. M. Olde Loohuis, M. Luciano, C. Macare, K. A.
763 Mather, M. Mattheisen, Y. Milaneschi, K. Nho, M. Papmeyer, A. Ramasamy, S. L. Risacher, R. Roiz-Santiañez, E. J.
764 Rose, A. Salami, P. G. Sämann, L. Schmaal, A. J. Schork, J. Shin, L. T. Strike, A. Teumer, M. M. J. van Donkelaar,
765 K. R. van Eijk, R. K. Walters, L. T. Westlye, C. D. Whelan, A. M. Winkler, M. P. Zwiers, S. Alhusaini, L. Athanasiu,
766 S. Ehrlich, M. M. H. Hakobjan, C. B. Hartberg, U. K. Haukvik, A. J. G. A. M. Heister, D. Hoehn, D. Kasperaviciute,
767 D. C. M. Liewald, L. M. Lopez, R. R. R. Makkinje, M. Matarin, M. A. M. Naber, D. Reese McKay, M. Needham, A.
768 C. Nugent, B. Pütz, N. A. Royle, L. Shen, E. Sprooten, D. Trabzuni, S. S. L. van der Marel, K. J. E. van Hulzen, E.
769 Walton, C. Wolf, L. Almasy, D. Ames, S. Arepalli, A. A. Assareh, M. E. Bastin, H. Brodaty, K. B. Bulayeva, M. A.
770 Carless, S. Cichon, A. Corvin, J. E. Curran, M. Czisch, G. I. de Zubizaray, A. Dillman, R. Duggirala, T. D. Dyer, S.
771 Erk, I. O. Fedko, L. Ferrucci, T. M. Foroud, P. T. Fox, M. Fukunaga, J. Raphael Gibbs, H. H. H. Göring, R. C. Green,
772 S. Guelfi, N. K. Hansell, C. A. Hartman, K. Hegenscheid, A. Heinz, D. G. Hernandez, D. J. Heslenfeld, P. J.
773 Hoekstra, F. Holsboer, G. Homuth, J.-J. Hottenga, M. Ikeda, C. R. Jack, M. Jenkinson, R. Johnson, R. Kanai, M.
774 Keil, J. W. Kent, P. Kochunov, J. B. Kwok, S. M. Lawrie, X. Liu, D. L. Longo, K. L. McMahon, E. Meisenzahl, I.
775 Melle, S. Mohnke, G. W. Montgomery, J. C. Mostert, T. W. Mühlleisen, M. A. Nalls, T. E. Nichols, L. G. Nilsson, M.
776 M. Nöthen, K. Ohi, R. L. Olvera, R. Perez-Iglesias, G. Bruce Pike, S. G. Potkin, I. Reinvang, S. Reppermund, M.
777 Rietschel, N. Romanczuk-Seiferth, G. D. Rosen, D. Rujescu, K. Schnell, P. R. Schofield, C. Smith, V. M. Steen, J. E.
778 Sussmann, A. Thalamuthu, A. W. Toga, B. J. Traynor, J. Troncoso, J. A. Turner, M. C. Valdés Hernández, D. van 't
779 Ent, M. van der Brug, N. J. A. van der Wee, M.-J. van Tol, D. J. Veltman, T. H. Wassink, E. Westman, R. H. Zielke,
780 A. B. Zonderman, D. G. Ashbrook, R. Hager, L. Lu, F. J. McMahon, D. W. Morris, R. W. Williams, H. G. Brunner,
781 R. L. Buckner, J. K. Buitelaar, W. Cahn, V. D. Calhoun, G. L. Cavalleri, B. Crespo-Facorro, A. M. Dale, G. E.
782 Davies, N. Delanty, C. Depondt, S. Djurovic, W. C. Drevets, T. Espeseth, R. L. Gollub, B.-C. Ho, W. Hoffmann, N.
783 Hosten, R. S. Kahn, S. Le Hellard, A. Meyer-Lindenberg, B. Müller-Myhsok, M. Nauck, L. Nyberg, M. Pandolfo, B.
784 W. J. H. Penninx, J. L. Roffman, S. M. Sisodiya, J. W. Smoller, H. van Bokhoven, N. E. M. van Haren, H. Völzke,
785 H. Walter, M. W. Weiner, W. Wen, T. White, I. Agartz, O. A. Andreassen, J. Blangero, D. I. Boomsma, R. M.
786 Brouwer, D. M. Cannon, M. R. Cookson, E. J. C. de Geus, I. J. Deary, G. Donohoe, G. Fernández, S. E. Fisher, C.
787 Francks, D. C. Glahn, H. J. Grabe, O. Gruber, J. Hardy, R. Hashimoto, H. E. Hulshoff Pol, E. G. Jönsson, I.
788 Kloszewska, S. Lovestone, V. S. Mattay, P. Mecocci, C. McDonald, A. M. McIntosh, R. A. Ophoff, T. Paus, Z.
789 Pausova, M. Ryten, P. S. Sachdev, A. J. Saykin, A. Simmons, A. Singleton, H. Soininen, J. M. Wardlaw, M. E.
790 Weale, D. R. Weinberger, H. H. H. Adams, L. J. Launer, S. Seiler, R. Schmidt, G. Chauhan, C. L. Satizabal, J. T.
791 Becker, L. Yanek, S. J. van der Lee, M. Ebbling, B. Fischl, W. T. Longstreth, D. Greve, H. Schmidt, P. Nyquist, L. N.
792 Vinke, C. M. van Duijn, L. Xue, B. Mazoyer, J. C. Bis, V. Gudnason, S. Seshadri, M. A. Ikram, N. G. Martin, M. J.
793 Wright, G. Schumann, B. Franke, P. M. Thompson, S. E. Medland, Common genetic variants influence human
794 subcortical brain structures. *Nature* **520**, 224–229 (2015).
795 4. C. L. Satizabal, H. H. H. Adams, D. P. Hibar, C. C. White, M. J. Knol, J. L. Stein, M. Scholz, M.
796 Sargurupremraj, N. Jahanshad, G. V. Roshchupkin, A. V. Smith, J. C. Bis, X. Jian, M. Luciano, E. Hofer, A. Teumer,
797 S. J. Van Der Lee, J. Yang, L. R. Yanek, T. V. Lee, S. Li, Y. Hu, J. Y. Koh, J. D. Eicher, S. Desrivière, A. Arias-
798 Vasquez, G. Chauhan, L. Athanasiu, M. E. Rentería, S. Kim, D. Hoehn, N. J. Armstrong, Q. Chen, A. J. Holmes, A.
799 Den Braber, I. Kloszewska, M. Andersson, T. Espeseth, O. Grimm, L. Abramovic, S. Alhusaini, Y. Milaneschi, M.
800 Papmeyer, T. Axelsson, S. Ehrlich, R. Roiz-Santiañez, B. Kraemer, A. K. Häberg, H. J. Jones, G. B. Pike, D. J. Stein,
801 A. Stevens, J. Bralten, M. W. Vernooij, T. B. Harris, I. Filippi, A. V. Witte, T. Guadalupe, K. Wittfeld, T. H. Mosley,
802 J. T. Becker, N. T. Doan, S. P. Hagenaars, Y. Saba, G. Cuellar-Partida, N. Amin, S. Hilal, K. Nho, N. Mirza-
803 Schreiber, K. Arfanakis, D. M. Becker, D. Ames, A. L. Goldman, P. H. Lee, D. I. Boomsma, S. Lovestone, S.
804 Giddaluru, S. Le Hellard, M. Mattheisen, M. M. Bohlken, D. Kasperaviciute, L. Schmaal, S. M. Lawrie, I. Agartz, E.
805 Walton, D. Tordesillas-Gutierrez, G. E. Davies, J. Shin, J. C. Ipser, L. N. Vinke, M. Hoogman, T. Jia, R. Burkhardt,
806 M. Klein, F. Crivello, D. Janowitz, O. Carmichael, U. K. Haukvik, B. S. Aribisala, H. Schmidt, L. T. Strike, C.-Y.
807 Cheng, S. L. Risacher, B. Pütz, D. A. Fleischman, A. A. Assareh, V. S. Mattay, R. L. Buckner, P. Mecocci, A. M.
808 Dale, S. Cichon, M. P. Boks, M. Matarin, B. W. J. H. Penninx, V. D. Calhoun, M. M. Chakravarty, A. F. Marquand,
809 C. Macare, S. Kharabian Masouleh, J. Oosterlaan, P. Amouyel, K. Hegenscheid, J. I. Rotter, A. J. Schork, D. C. M.

- 810 Liewald, G. I. De Zubicaray, T. Y. Wong, L. Shen, P. G. Sämann, H. Brodaty, J. L. Roffman, E. J. C. De Geus, M.
811 Tsolaki, S. Erk, K. R. Van Eijk, G. L. Cavalleri, N. J. A. Van Der Wee, A. M. McIntosh, R. L. Gollub, K. B.
812 Bulayeva, M. Bernard, J. S. Richards, J. J. Himali, M. Loeffler, N. Rommelse, W. Hoffmann, L. T. Westlye, M. C.
813 Valdés Hernández, N. K. Hansell, T. G. M. Van Erp, C. Wolf, J. B. J. Kwok, B. Vellas, A. Heinz, L. M. Olde
814 Loohuis, N. Delanty, B.-C. Ho, C. R. K. Ching, E. Shumskaya, B. Singh, A. Hofman, D. Van Der Meer, G. Homuth,
815 B. M. Psaty, M. E. Bastin, G. W. Montgomery, T. M. Foroud, S. Reppermund, J.-J. Hottenga, A. Simmons, A.
816 Meyer-Lindenberg, W. Cahn, C. D. Whelan, M. M. J. Van Donkelaar, Q. Yang, N. Hosten, R. C. Green, A.
817 Thalamuthu, S. Mohnke, H. E. Hulshoff Pol, H. Lin, C. R. Jack, P. R. Schofield, T. W. Mühlleisen, P. Maillard, S. G.
818 Potkin, W. Wen, E. Fletcher, A. W. Toga, O. Gruber, M. Huentelman, G. Davey Smith, L. J. Launer, L. Nyberg, E.
819 G. Jönsson, B. Crespo-Facorro, N. Koen, D. N. Greve, A. G. Uitterlinden, D. R. Weinberger, V. M. Steen, I. O.
820 Fedko, N. A. Groenewold, W. J. Niessen, R. Toro, C. Tzourio, W. T. Longstreth, M. K. Ikram, J. W. Smoller, M.-J.
821 Van Tol, J. E. Sussmann, T. Paus, H. Lemaître, M. L. Schroeter, B. Mazoyer, O. A. Andreassen, F. Holsboer, C.
822 Depondt, D. J. Veltman, J. A. Turner, Z. Pausova, G. Schumann, D. Van Rooij, S. Djurovic, I. J. Deary, K. L.
823 McMahon, B. Müller-Myhsok, R. M. Brouwer, H. Soininen, M. Pandolfo, T. H. Wassink, J. W. Cheung, T. Wolfers,
824 J.-L. Martinot, M. P. Zwiers, M. Nauck, I. Melle, N. G. Martin, R. Kanai, E. Westman, R. S. Kahn, S. M. Sisodiya, T.
825 White, A. Saremi, H. Van Bokhoven, H. G. Brunner, H. Völzke, M. J. Wright, D. Van 'T Ent, M. M. Nöthen, R. A.
826 Ophoff, J. K. Buitelaar, G. Fernández, P. S. Sachdev, M. Rietschel, N. E. M. Van Haren, S. E. Fisher, A. S. Beiser, C.
827 Francks, A. J. Saykin, K. A. Mather, N. Romanczuk-Seiferth, C. A. Hartman, A. L. DeStefano, D. J. Heslenfeld, M.
828 W. Weiner, H. Walter, P. J. Hoekstra, P. A. Nyquist, B. Franke, D. A. Bennett, H. J. Grabe, A. D. Johnson, C. Chen,
829 C. M. Van Duijn, O. L. Lopez, M. Fornage, J. M. Wardlaw, R. Schmidt, C. DeCarli, P. L. De Jager, A. Villringer, S.
830 Debette, V. Gudnason, S. E. Medland, J. M. Shulman, P. M. Thompson, S. Seshadri, M. A. Ikram, Genetic
831 architecture of subcortical brain structures in 38,851 individuals. *Nat Genet* **51**, 1624–1636 (2019).
832 5. T. Elvsåshagen, S. Bahrami, D. Van Der Meer, I. Agartz, D. Alnæs, D. M. Barch, R. Baur-Streubel, A.
833 Bertolino, M. K. Beyer, G. Blasi, S. Borgwardt, B. Boye, J. Buitelaar, E. Bøen, E. G. Celius, S. Cervenka, A.
834 Conzelmann, D. Coynel, P. Di Carlo, S. Djurovic, S. Eisenacher, T. Espeseth, H. Fatouros-Bergman, L. Flyckt, B.
835 Franke, O. Frei, B. Gelao, H. F. Harbo, C. A. Hartman, A. Håberg, D. Heslenfeld, P. J. Hoekstra, E. A. Høgestøl, R.
836 Jonassen, E. G. Jönsson, Karolinska Schizophrenia Project (KaSP) consortium, L. Farde, L. Flyckt, G. Engberg, S.
837 Erhardt S. H. Fatouros-Bergman, S. Cervenka, L. Schwieder, F. Piehl, I. Agartz, K. Collste, P. Victorsson, A.
838 Malmqvist, M. Hedberg, F. Orhan, C. M. Sellgren, P. Kirsch, I. Kłoszewska, T. V. Lagerberg, N. I. Landrø, S. Le
839 Hellard, K.-P. Lesch, L. A. Maglanoc, U. F. Malt, P. Mecocci, I. Melle, A. Meyer-Lindenberg, T. Moberget, J. E.
840 Nordvik, L. Nyberg, K. S. O. Connell, J. Oosterlaan, M. Papalino, A. Papassotiropoulos, P. Pauli, G. Pergola, K.
841 Persson, D. De Quervain, A. Reif, J. Rokicki, D. Van Rooij, A. A. Shadrin, A. Schmidt, E. Schwarz, G. Selbæk, H.
842 Soininen, P. Sowa, V. M. Steen, M. Tsolaki, B. Vellas, L. Wang, E. Westman, G. C. Ziegler, M. Zink, O. A.
843 Andreassen, L. T. Westlye, T. Kaufmann, The genetic architecture of human brainstem structures and their
844 involvement in common brain disorders. *Nat Commun* **11**, 4016 (2020).
845 6. T. Ge, M. Reuter, A. M. Winkler, A. J. Holmes, P. H. Lee, L. S. Tirrell, J. L. Roffman, R. L. Buckner, J. W.
846 Smoller, M. R. Sabuncu, Multidimensional heritability analysis of neuroanatomical shape. *Nat Commun* **7**, 13291
847 (2016).
848 7. G. V. Roshchupkin, B. A. Gutman, M. W. Vernooij, N. Jahanshad, N. G. Martin, A. Hofman, K. L.
849 McMahon, S. J. Van Der Lee, C. M. Van Duijn, G. I. De Zubicaray, A. G. Uitterlinden, M. J. Wright, W. J. Niessen,
850 P. M. Thompson, M. A. Ikram, H. H. H. Adams, Heritability of the shape of subcortical brain structures in the
851 general population. *Nat Commun* **7**, 13738 (2016).
852 8. B. A. Gutman, T. G. M. Van Erp, K. Alpert, C. R. K. Ching, D. Isaev, A. Ragothaman, N. Jahanshad, A.
853 Saremi, A. Zavaliangos-Petropulu, D. C. Glahn, L. Shen, S. Cong, D. Alnæs, O. A. Andreassen, N. T. Doan, L. T.
854 Westlye, P. Kochunov, T. D. Satterthwaite, D. H. Wolf, A. J. Huang, C. Kessler, A. Weideman, D. Nguyen, B. A.
855 Mueller, L. Faziola, S. G. Potkin, A. Preda, D. H. Mathalon, J. Bustillo, V. Calhoun, J. M. Ford, E. Walton, S.
856 Ehrlich, G. Ducci, N. Banaj, F. Piras, F. Piras, G. Spalletta, E. J. Canales-Rodríguez, P. Fuentes-Claramonte, E.
857 Pomarol-Clotet, J. Radua, R. Salvador, S. Sarró, E. W. Dickie, A. Voineskos, D. Tordesillas-Gutiérrez, B. Crespo-
858 Facorro, E. Setién-Suero, J. M. Van Son, S. Borgwardt, F. Schönborn-Harrisberger, D. Morris, G. Donohoe, L.
859 Holleran, D. Cannon, C. McDonald, A. Corvin, M. Gill, G. B. Filho, P. G. P. Rosa, M. H. Serpa, M. V. Zanetti, I.
860 Lebedeva, V. Kaleda, A. Tomyshev, T. Crow, A. James, S. Cervenka, C. M. Sellgren, H. Fatouros-Bergman, I.
861 Agartz, F. Howells, D. J. Stein, H. Temmingh, A. Uhmann, G. I. De Zubicaray, K. L. McMahon, M. Wright, D.
862 Cobia, J. G. Csernansky, P. M. Thompson, J. A. Turner, L. Wang, A META-ANALYSIS of deep brain structural shape
863 and asymmetry abnormalities in 2,833 individuals with schizophrenia compared with 3,929 healthy volunteers via the
864 ENIGMA CONSORTIUM. *Human Brain Mapping* **43**, 352–372 (2022).
865 9. L. T. Elliott, K. Sharp, F. Alfaro-Almagro, S. Shi, K. L. Miller, G. Douaud, J. Marchini, S. M. Smith,
866 Genome-wide association studies of brain imaging phenotypes in UK Biobank. *Nature* **562**, 210–216 (2018).
867 10. C. C. Fan, R. Loughnan, C. Makowski, D. Pecheva, C.-H. Chen, D. J. Hagler, W. K. Thompson, N. Parker,
868 D. van der Meer, O. Frei, O. A. Andreassen, A. M. Dale, Multivariate genome-wide association study on tissue-
869 sensitive diffusion metrics highlights pathways that shape the human brain. *Nat Commun* **13**, 2423 (2022).
870 11. S. Goovaerts, H. Hoskens, R. J. Eller, N. Herrick, A. M. Musolf, C. M. Justice, M. Yuan, S. Naqvi, M. K.

- 871 Lee, D. Vandermeulen, H. L. Szabo-Rogers, P. A. Romitti, S. A. Boyadjiev, M. L. Marazita, J. R. Shaffer, M. D.
872 Shriver, J. Wysocka, S. Walsh, S. M. Weinberg, P. Claes, Joint multi-ancestry and admixed GWAS reveals the
873 complex genetics behind human cranial vault shape. *Nat Commun* **14**, 7436 (2023).
- 874 12. S. Naqvi, Y. Slep, H. Hoskens, K. Indencleef, J. P. Spence, R. Bruffaerts, A. Radwan, R. J. Eller, S.
875 Richmond, M. D. Shriner, J. R. Shaffer, S. M. Weinberg, S. Walsh, J. Thompson, J. K. Pritchard, S. Sunaert, H.
876 Peeters, J. Wysocka, P. Claes, Shared heritability of human face and brain shape. *Nat Genet* **53**, 830–839 (2021).
- 877 13. M. Reuter, F.-E. Wolter, N. Peinecke, Laplace–Beltrami spectra as ‘Shape-DNA’ of surfaces and solids.
878 *Computer-Aided Design* **38**, 342–366 (2006).
- 879 14. M. Reuter, F.-E. Wolter, N. Peinecke, “Laplace-spectra as fingerprints for shape matching” in *Proceedings
880 of the 2005 ACM Symposium on Solid and Physical Modeling* (ACM, Cambridge Massachusetts, 2005;
881 <https://dl.acm.org/doi/10.1145/1060244.1060256>), pp. 101–106.
- 882 15. E. F. F. Chladni, *Entdeckungen über die Theorie des Klanges* (bey Weidmanns Erben und Reich, 1787;
883 <https://www.e-rara.ch/zut/doi/10.3931/e-rara-4235>).
- 884 16. M. Kac, Can One Hear the Shape of a Drum? *The American Mathematical Monthly* **73**, 1 (1966).
- 885 17. C. Gordon, D. L. Webb, S. Wolpert, One cannot hear the shape of a drum. *Bull. Amer. Math. Soc.* **27**, 134–
886 138 (1992).
- 887 18. S. Zelditch, Inverse spectral problem for analytic domains, II: \mathbb{Z}_2 -symmetric domains. *Ann. Math.* **170**,
888 205–269 (2009).
- 889 19. M. Reuter, F.-E. Wolter, M. Shenton, M. Niethammer, Laplace–Beltrami eigenvalues and topological
890 features of eigenfunctions for statistical shape analysis. *Computer-Aided Design* **41**, 739–755 (2009).
- 891 20. H. P. McKean, Jr., I. M. Singer, Curvature and the eigenvalues of the Laplacian. *J. Differential Geom.* **1**
892 (1967).
- 893 21. C. Wachinger, P. Golland, W. Kremen, B. Fischl, M. Reuter, BrainPrint: A discriminative characterization
894 of brain morphology. *NeuroImage* **109**, 232–248 (2015).
- 895 22. M. Niethammer, M. Reuter, F.-E. Wolter, S. Bouix, N. Peinecke, M.-S. Koo, M. E. Shenton, “Global
896 Medical Shape Analysis Using the Laplace–Beltrami Spectrum” in *Medical Image Computing and Computer-Assisted
897 Intervention – MICCAI 2007*, N. Ayache, S. Ourselin, A. Maeder, Eds. (Springer Berlin Heidelberg, Berlin,
898 Heidelberg, 2007; http://link.springer.com/10.1007/978-3-540-75757-3_103) vol. 4791 of *Lecture Notes in Computer
899 Science*, pp. 850–857.
- 900 23. J. C. Pang, K. M. Aquino, M. Oldehinkel, P. A. Robinson, B. D. Fulcher, M. Breakspear, A. Fornito,
901 Geometric constraints on human brain function. *Nature* **618**, 566–574 (2023).
- 902 24. D. Van Der Meer, A. A. Shadrin, K. O’Connell, F. Bettella, S. Djurovic, T. Wolfers, D. Alnæs, I. Agartz, O.
903 B. Smeland, I. Melle, J. M. Sánchez, D. E. J. Linden, A. M. Dale, L. T. Westlye, O. A. Andreassen, O. Frei, T.
904 Kaufmann, Boosting Schizophrenia Genetics by Utilizing Genetic Overlap With Brain Morphology. *Biological
905 Psychiatry* **92**, 291–298 (2022).
- 906 25. S. Bahrami, K. Nordengen, A. A. Shadrin, O. Frei, D. Van Der Meer, A. M. Dale, L. T. Westlye, O. A.
907 Andreassen, T. Kaufmann, Distributed genetic architecture across the hippocampal formation implies common
908 neuropathology across brain disorders. *Nat Commun* **13**, 3436 (2022).
- 909 26. T. Elvsåshagen, A. Shadrin, O. Frei, D. Van Der Meer, S. Bahrami, V. J. Kumar, O. Smeland, L. T. Westlye,
910 O. A. Andreassen, T. Kaufmann, The genetic architecture of the human thalamus and its overlap with ten common
911 brain disorders. *Nat Commun* **12**, 2909 (2021).
- 912 27. H. H. Yin, B. J. Knowlton, The role of the basal ganglia in habit formation. *Nat Rev Neurosci* **7**, 464–476
913 (2006).
- 914 28. L. T. Grinberg, U. Rueb, H. Heinzen, Brainstem: Neglected Locus in Neurodegenerative Diseases. *Front.
915 Neur.* **2** (2011).
- 916 29. K. Watanabe, E. Taskesen, A. van Bochoven, D. Posthuma, Functional mapping and annotation of genetic
917 associations with FUMA. *Nat Commun* **8**, 1826 (2017).
- 918 30. K. Wang, M. Li, H. Hakonarson, ANNOVAR: functional annotation of genetic variants from high-
919 throughput sequencing data. *Nucleic Acids Research* **38**, e164 (2010).
- 920 31. M. Kircher, D. M. Witten, P. Jain, B. J. O’Roak, G. M. Cooper, J. Shendure, A general framework for
921 estimating the relative pathogenicity of human genetic variants. *Nat Genet* **46**, 310–315 (2014).
- 922 32. M. J. Landrum, S. Chitipiralla, G. R. Brown, C. Chen, B. Gu, J. Hart, D. Hoffman, W. Jang, K. Kaur, C. Liu,
923 V. Lyoshin, Z. Maddipatla, R. Maiti, J. Mitchell, N. O’Leary, G. R. Riley, W. Shi, G. Zhou, V. Schneider, D.
924 Maglott, J. B. Holmes, B. L. Kattman, ClinVar: improvements to accessing data. *Nucleic Acids Res* **48**, D835–D844
925 (2020).
- 926 33. J. Cheng, G. Novati, J. Pan, C. Bycroft, A. Žemgulytė, T. Applebaum, A. Pritchel, L. H. Wong, M. Zielinski,
927 T. Sargeant, R. G. Schneider, A. W. Senior, J. Jumper, D. Hassabis, P. Kohli, Ž. Avsec, Accurate proteome-wide
928 missense variant effect prediction with AlphaMissense. *Science* **381**, eadg7492 (2023).
- 929 34. Schizophrenia Working Group of the Psychiatric Genomics Consortium, Biological insights from 108
930 schizophrenia-associated genetic loci. *Nature* **511**, 421–427 (2014).
- 931 35. N. Carrera, M. Arrojo, J. Sanjuán, R. Ramos-Ríos, E. Paz, J. J. Suárez-Rama, M. Páramo, S. Agra, J.

- 932 Brenlla, S. Martínez, O. Rivero, D. A. Collier, A. Palotie, S. Cichon, M. M. Nöthen, M. Rietschel, D. Rujescu, H.
933 Stefansson, S. Steinberg, E. Sigurdsson, D. St. Clair, S. Tosato, T. Werge, K. Stefansson, J. C. González, J. Valero,
934 A. Gutiérrez-Zotes, A. Labad, L. Martorell, E. Vilella, Á. Carracedo, J. Costas, Association Study of
935 Nonsynonymous Single Nucleotide Polymorphisms in Schizophrenia. *Biological Psychiatry* **71**, 169–177 (2012).
- 936 36. GERAD1 Consortium, CRESTAR Consortium, A. F. Pardiñas, P. Holmans, A. J. Pocklington, V. Escott-
937 Price, S. Ripke, N. Carrera, S. E. Legge, S. Bishop, D. Cameron, M. L. Hamshere, J. Han, L. Hubbard, A. Lynham,
938 K. Mantripragada, E. Rees, J. H. MacCabe, S. A. McCarroll, B. T. Baune, G. Breen, E. M. Byrne, U. Dannlowski, T.
939 C. Eley, C. Hayward, N. G. Martin, A. M. McIntosh, R. Plomin, D. J. Porteous, N. R. Wray, A. Caballero, D. H.
940 Geschwind, L. M. Huckins, D. M. Ruderfer, E. Santiago, P. Sklar, E. A. Stahl, H. Won, E. Agerbo, T. D. Als, O. A.
941 Andreassen, M. Bækvad-Hansen, P. B. Mortensen, C. B. Pedersen, A. D. Børglum, J. Bybjerg-Grauholt, S.
942 Djurovic, N. Durmishi, M. G. Pedersen, V. Golimbet, J. Grove, D. M. Hougaard, M. Mattheisen, E. Molden, O.
943 Mors, M. Nordentoft, M. Pejovic-Milovancevic, E. Sigurdsson, T. Silagadze, C. S. Hansen, K. Stefansson, H.
944 Stefansson, S. Steinberg, S. Tosato, T. Werge, D. A. Collier, D. Rujescu, G. Kirov, M. J. Owen, M. C. O'Donovan, J.
945 T. R. Walters, Common schizophrenia alleles are enriched in mutation-intolerant genes and in regions under strong
946 background selection. *Nat Genet* **50**, 381–389 (2018).
- 947 37. D. Li, J.-P. Achkar, T. Haritunians, J. P. Jacobs, K. Y. Hui, M. D'Amato, S. Brand, G. Radford-Smith, J.
948 Halfvarson, J.-H. Niess, S. Kugathasan, C. Büning, L. P. Schumm, L. Klei, A. Ananthakrishnan, G. Aumais, L.
949 Baidoo, M. Dubinsky, C. Fiocchi, J. Glas, R. Milgrom, D. D. Proctor, M. Regueiro, L. A. Simms, J. M. Stempak, S.
950 R. Targan, L. Törkvist, Y. Sharma, B. Devlin, J. Borneman, H. Hakonarson, R. J. Xavier, M. Daly, S. R. Brant, J. D.
951 Rioux, M. S. Silverberg, J. H. Cho, J. Braun, D. P. McGovern, R. H. Duerr, A pleiotropic missense variant in
952 SLC39A8 is associated with Crohn's disease and human gut microbiome composition. *Gastroenterology* **151**, 724–
953 732 (2016).
- 954 38. The International Consortium for Blood Pressure Genome-Wide Association Studies., Genetic Variants in
955 Novel Pathways Influence Blood Pressure and Cardiovascular Disease Risk. *Nature* **478**, 103–109 (2011).
- 956 39. T. M. Caffrey, R. Wade-Martins, Functional MAPT haplotypes: Bridging the gap between genotype and
957 neuropathology. *Neurobiology of Disease* **27**, 1–10 (2007).
- 958 40. M. Wainberg, N. J. Forde, S. Mansour, I. Kerrebijn, S. E. Medland, C. Hawco, S. J. Tripathy, Genetic
959 architecture of the structural connectome. *Nat Commun* **15**, 1962 (2024).
- 960 41. C. A. de Leeuw, J. M. Mooij, T. Heskes, D. Posthuma, MAGMA: Generalized Gene-Set Analysis of GWAS
961 Data. *PLOS Computational Biology* **11**, e1004219 (2015).
- 962 42. T. Rittman, M. Rubinov, P. E. Vértes, A. X. Patel, C. E. Ginestet, B. C. P. Ghosh, R. A. Barker, M. G.
963 Spillantini, E. T. Bullmore, J. B. Rowe, Regional expression of the MAPT gene is associated with loss of hubs in
964 brain networks and cognitive impairment in Parkinson disease and progressive supranuclear palsy. *Neurobiology of
965 Aging* **48**, 153–160 (2016).
- 966 43. R. S. Desikan, A. J. Schork, Y. Wang, A. Witoelar, M. Sharma, L. K. McEvoy, D. Holland, J. B. Brewer,
967 C.-H. Chen, W. K. Thompson, D. Harold, J. Williams, M. J. Owen, M. C. O'Donovan, M. A. Pericak-Vance, R.
968 Mayeux, J. L. Haines, L. A. Farrer, G. D. Schellenberg, P. Heutink, A. B. Singleton, A. Brice, N. W. Wood, J. Hardy,
969 M. Martinez, S. H. Choi, A. DeStefano, M. A. Ikram, J. C. Bis, A. Smith, A. L. Fitzpatrick, L. Launer, C. Van Duijn,
970 S. Seshadri, I. D. Ulstein, D. Aarsland, T. Fladby, S. Djurovic, B. T. Hyman, J. Snaedal, H. Stefansson, K.
971 Stefansson, T. Gasser, O. A. Andreassen, A. M. Dale, for the ADNI ADGC, GERAD, CHARGE and IPDGC
972 Investigators, Genetic overlap between Alzheimer's disease and Parkinson's disease at the MAPT locus. *Mol
973 Psychiatry* **20**, 1588–1595 (2015).
- 974 44. E. M. Weeks, J. C. Ulirsch, N. Y. Cheng, B. L. Trippe, R. S. Fine, J. Miao, T. A. Patwardhan, M. Kanai, J.
975 Nasser, C. P. Fulco, K. C. Tashman, F. Aguet, T. Li, J. Ordovas-Montanes, C. S. Smillie, M. Biton, A. K. Shalek, A.
976 N. Ananthakrishnan, R. J. Xavier, A. Regev, R. M. Gupta, K. Lage, K. G. Ardlie, J. N. Hirschhorn, E. S. Lander, J.
977 M. Engreitz, H. K. Finucane, Leveraging polygenic enrichments of gene features to predict genes underlying
978 complex traits and diseases. *Nat Genet* **55**, 1267–1276 (2023).
- 979 45. Z. Sha, D. Schijven, S. E. Fisher, C. Francks, Genetic architecture of the white matter connectome of the
980 human brain. *SCIENCE ADVANCES* (2023).
- 981 46. Y. Benjamini, Y. Hochberg, Controlling the False Discovery Rate: A Practical and Powerful Approach to
982 Multiple Testing. *Journal of the Royal Statistical Society: Series B (Methodological)* **57**, 289–300 (1995).
- 983 47. Y. Wu, K. S. Burch, A. Ganna, P. Pajukanta, B. Pasaniuc, S. Sankararaman, Fast estimation of genetic
984 correlation for biobank-scale data. *The American Journal of Human Genetics* **109**, 24–32 (2022).
- 985 48. C. Palmer, I. Pe'er, Statistical correction of the Winner's Curse explains replication variability in
986 quantitative trait genome-wide association studies. *PLoS Genet* **13**, e1006916 (2017).
- 987 49. D. van der Meer, J. Rokicki, T. Kaufmann, A. Córdova-Palomera, T. Moberget, D. Alnæs, F. Bettella, O.
988 Frei, N. T. Doan, I. E. Sønderby, O. B. Smeland, I. Agartz, A. Bertolino, J. Bralten, C. L. Brandt, J. K. Buitelaar, S.
989 Djurovic, M. van Donkelaar, E. S. Dørrum, T. Espeseth, S. V. Faraone, G. Fernández, S. E. Fisher, B. Franke, B.
990 Haatveit, C. A. Hartman, P. J. Hoekstra, A. K. Häberg, E. G. Jönsson, K. K. Kolskår, S. Le Hellard, M. J. Lund, A. J.
991 Lundervold, A. Lundervold, I. Melle, J. Monereo Sánchez, L. C. Norbom, J. E. Nordvik, L. Nyberg, J. Oosterlaan, M.
992 Papalino, A. Papassotiropoulos, G. Pergola, D. J. F. de Quervain, G. Richard, A.-M. Sanders, P. Selvaggi, E.

- 993 Shumskaya, V. M. Steen, S. Tønnesen, K. M. Ulrichsen, M. P. Zwiers, O. A. Andreassen, L. T. Westlye, Brain scans
994 from 21,297 individuals reveal the genetic architecture of hippocampal subfield volumes. *Mol Psychiatry* **25**, 3053–
995 3065 (2020).
- 996 50. M. Lanfranchi, S. Yandiev, G. Meyer-Dilhet, S. Ellouze, M. Kerkhofs, R. Dos Reis, A. Garcia, C. Blondet,
997 A. Amar, A. Kneppers, H. Polvèche, D. Plassard, M. Foretz, B. Viollet, K. Sakamoto, R. Mounier, C. F. Bourgeois,
998 O. Raineteau, E. Goillot, J. Courchet, The AMPK-related kinase NUAK1 controls cortical axons branching by locally
999 modulating mitochondrial metabolic functions. *Nat Commun* **15**, 2487 (2024).
- 1000 51. C. Makowski, H. Wang, A. Srinivasan, A. Qi, Y. Qiu, D. van der Meer, O. Frei, J. Zou, P. M. Visscher, J.
1001 Yang, C.-H. Chen, Larger cerebral cortex is genetically correlated with greater frontal area and dorsal thickness.
1002 *Proceedings of the National Academy of Sciences* **120**, e2214834120 (2023).
- 1003 52. A. Okbay, Y. Wu, N. Wang, H. Jayashankar, M. Bennett, S. M. Nezhati, J. Sidorenko, H. Kweon, G.
1004 Goldman, T. Gjorgjieva, Y. Jiang, B. Hicks, C. Tian, D. A. Hinds, R. Ahlskog, P. K. E. Magnusson, S. Oskarsson, C.
1005 Hayward, A. Campbell, D. J. Porteous, J. Freese, P. Herd, C. Watson, J. Jala, D. Conley, P. D. Koellinger, M.
1006 Johannesson, D. Laibson, M. N. Meyer, J. J. Lee, A. Kong, L. Yengo, D. Cesarini, P. Turley, P. M. Visscher, J. P.
1007 Beauchamp, D. J. Benjamin, A. I. Young, Polygenic prediction of educational attainment within and between
1008 families from genome-wide association analyses in 3 million individuals. *Nat Genet* **54**, 437–449 (2022).
- 1009 53. M. P. M. Soutar, D. Melandri, B. O'Callaghan, E. Annuario, A. E. Monaghan, N. J. Welsh, K. D'Sa, S.
1010 Guelfi, D. Zhang, A. Pittman, D. Trabzuni, A. H. A. Verboven, K. S. Pan, D. A. Kia, M. Bictash, S. Gandhi, H.
1011 Houlden, M. R. Cookson, N. N. Kasri, N. W. Wood, A. B. Singleton, J. Hardy, P. J. Whiting, C. Blauwendraat, A. J.
1012 Whitworth, C. Manzoni, M. Ryten, P. A. Lewis, H. Plun-Favreau, Regulation of mitophagy by the NSL complex
1013 underlies genetic risk for Parkinson's disease at 16q11.2 and MAPT H1 loci. *Brain* **145**, 4349–4367 (2022).
- 1014 54. M. Baker, I. Litvan, H. Houlden, J. Adamson, D. Dickson, J. Perez-Tur, J. Hardy, T. Lynch, E. Bigio, M.
1015 Hutton, Association of an Extended Haplotype in the Tau Gene with Progressive Supranuclear Palsy. *Human
1016 Molecular Genetics* **8**, 711–715 (1999).
- 1017 55. A. M. Pittman, The structure of the tau haplotype in controls and in progressive supranuclear palsy. *Human
1018 Molecular Genetics* **13**, 1267–1274 (2004).
- 1019 56. A. M. Pittman, A. J. Myers, P. Abou-Sleiman, H. C. Fung, M. Kaleem, L. Marlowe, J. Duckworth, D.
1020 Leung, D. Williams, L. Kilford, N. Thomas, C. M. Morris, D. Dickson, N. W. Wood, J. Hardy, A. J. Lees, R. de
1021 Silva, Linkage disequilibrium fine mapping and haplotype association analysis of the tau gene in progressive
1022 supranuclear palsy and corticobasal degeneration. *Journal of Medical Genetics* **42**, 837–846 (2005).
- 1023 57. P. Pastor, M. Ezquerre, J. C. Perez, S. Chakraverty, J. Norton, B. A. Racette, D. McKeel, J. S. Perlmuter, E.
1024 Tolosa, A. M. Goate, Novel haplotypes in 17q21 are associated with progressive supranuclear palsy. *Annals of
1025 Neurology* **56**, 249–258 (2004).
- 1026 58. M. G. Spillantini, J. R. Murrell, M. Goedert, M. R. Farlow, A. Klug, B. Ghetti, Mutation in the tau gene in
1027 familial multiple system tauopathy with presenile dementia. *Proceedings of the National Academy of Sciences* **95**,
1028 7737–7741 (1998).
- 1029 59. J. Simón-Sánchez, C. Schulte, J. M. Bras, M. Sharma, J. R. Gibbs, D. Berg, C. Paisan-Ruiz, P. Lichtner, S.
1030 W. Scholz, D. G. Hernandez, R. Krüger, M. Federoff, C. Klein, A. Goate, J. Perlmuter, M. Bonin, M. A. Nalls, T.
1031 Illig, C. Gieger, H. Houlden, M. Steffens, M. S. Okun, B. A. Racette, M. R. Cookson, K. D. Foote, H. H. Fernandez,
1032 B. J. Traynor, S. Schreiber, S. Arepalli, R. Zonozi, K. Gwinn, M. van der Brug, G. Lopez, S. J. Chanock, A.
1033 Schatzkin, Y. Park, A. Hollenbeck, J. Gao, X. Huang, N. W. Wood, D. Lorenz, G. Deuschl, H. Chen, O. Riess, J. A.
1034 Hardy, A. B. Singleton, T. Gasser, Genome-wide association study reveals genetic risk underlying Parkinson's
1035 disease. *Nat Genet* **41**, 1308–1312 (2009).
- 1036 60. P. Sánchez-Juan, S. Moreno, I. de Rojas, I. Hernández, S. Valero, M. Alegret, L. Montreal, P. García
1037 González, C. Lage, S. López-García, E. Rodríguez-Rodríguez, A. Orellana, L. Tárraga, M. Boada, A. Ruiz, The
1038 MAPT H1 Haplotype Is a Risk Factor for Alzheimer's Disease in APOE ε4 Non-carriers. *Front Aging Neurosci* **11**,
1039 327 (2019).
- 1040 61. N. Kouri, O. A. Ross, B. Dombroski, C. S. Younkin, D. J. Serie, A. Soto-Ortolaza, M. Baker, N. C. A.
1041 Finch, H. Yoon, J. Kim, S. Fujioka, C. A. McLean, B. Ghetti, S. Spina, L. B. Cantwell, M. R. Farlow, J. Grafman, E.
1042 D. Huey, M. Ryung Han, S. Beecher, E. T. Geller, H. A. Kretzschmar, S. Roeber, M. Gearing, J. L. Juncos, J. P. G.
1043 Vonsattel, V. M. Van Deerlin, M. Grossman, H. I. Hurtig, R. G. Gross, S. E. Arnold, J. Q. Trojanowski, V. M. Lee,
1044 G. K. Wenning, C. L. White, G. U. Höglinder, U. Müller, B. Devlin, L. I. Golbe, J. Crook, J. E. Parisi, B. F. Boeve,
1045 K. A. Josephs, Z. K. Wszolek, R. J. Uitti, N. R. Graff-Radford, I. Litvan, S. G. Younkin, L.-S. Wang, N. Ertekin-
1046 Taner, R. Rademakers, H. Hakonarsen, G. D. Schellenberg, D. W. Dickson, Genome-wide association study of
1047 corticobasal degeneration identifies risk variants shared with progressive supranuclear palsy. *Nat Commun* **6**, 7247
1048 (2015).
- 1049 62. C. Bellenguez, F. Küçükali, I. E. Jansen, L. Kleineidam, S. Moreno-Grau, N. Amin, A. C. Naj, R. Campos-
1050 Martin, B. Grenier-Boley, V. Andrade, P. A. Holmans, A. Boland, V. Damotte, S. J. van der Lee, M. R. Costa, T.
1051 Kuulasmaa, Q. Yang, I. de Rojas, J. C. Bis, A. Yaqub, I. Prokic, J. Chapuis, S. Ahmad, V. Giedraitis, D. Aarsland, P.
1052 Garcia-Gonzalez, C. Abdelnour, E. Alarcón-Martín, D. Alcolea, M. Alegret, I. Alvarez, V. Álvarez, N. J. Armstrong,
1053 A. Tsolaki, C. Antúnez, I. Appollonio, M. Arcaro, S. Archetti, A. A. Pastor, B. Arosio, L. Athanasiu, H. Baily, N.

- 1054 Banaj, M. Baquero, S. Barral, A. Beiser, A. B. Pastor, J. E. Below, P. Benchek, L. Benussi, C. Berr, C. Besse, V.
1055 Bessi, G. Binetti, A. Bizarro, R. Blesa, M. Boada, E. Boerwinkle, B. Borroni, S. Boschi, P. Bossù, G. Bråthen, J.
1056 Bressler, C. Bresner, H. Brodaty, K. J. Brookes, L. I. Brusco, D. Buiza-Rueda, K. Bürger, V. Burholt, W. S. Bush, M.
1057 Calero, L. B. Cantwell, G. Chene, J. Chung, M. L. Cuccaro, Á. Carracedo, R. Cecchetti, L. Cervera-Carles, C.
1058 Charbonnier, H.-H. Chen, C. Chillotti, S. Ciccone, J. A. H. R. Claassen, C. Clark, E. Conti, A. Corma-Gómez, E.
1059 Costantini, C. Custodero, D. Daian, M. C. Dalmasso, A. Daniele, E. Dardiots, J.-F. Dartigues, P. P. de Deyn, K. de
1060 Paiva Lopes, L. D. de Witte, S. Debette, J. Deckert, T. del Ser, N. Denning, A. DeStefano, M. Dichgans, J. Diehl-
1061 Schmid, M. Diez-Fairen, P. D. Rossi, S. Djurovic, E. Duron, E. Düzel, C. Dufouil, G. Eiriksdottir, S. Engelborghs, V.
1062 Escott-Price, A. Espinosa, M. Ewers, K. M. Faber, T. Fabrizio, S. F. Nielsen, D. W. Fardo, L. Farotti, C. Fenoglio,
1063 M. Fernández-Fuertes, R. Ferrari, C. B. Ferreira, E. Ferri, B. Fin, P. Fischer, T. Fladby, K. Fließbach, B. Fongang, M.
1064 Fornage, J. Fortea, T. M. Foroud, S. Fostinelli, N. C. Fox, E. Franco-Macías, M. J. Bullido, A. Frank-García, L.
1065 Froelich, B. Fulton-Howard, D. Galimberti, J. M. García-Alberca, P. García-González, S. Garcia-Madrona, G.
1066 Garcia-Ribas, R. Ghidoni, I. Giegling, G. Giorgio, A. M. Goate, O. Goldhardt, D. Gomez-Fonseca, A. González-
1067 Pérez, C. Graff, G. Grande, E. Green, T. Grimmer, E. Grünblatt, M. Grunin, V. Gudnason, T. Guetta-Baranes, A.
1068 Haapasalo, G. Hadjigeorgiou, J. L. Haines, K. L. Hamilton-Nelson, H. Hampel, O. Hanon, J. Hardy, A. M.
1069 Hartmann, L. Hausner, J. Harwood, S. Heilmann-Heimbach, S. Helisalmi, M. T. Heneka, I. Hernández, M. J.
1070 Herrmann, P. Hoffmann, C. Holmes, H. Holstege, R. H. Vilas, M. Hulsman, J. Humphrey, G. J. Biessels, X. Jian, C.
1071 Johansson, G. R. Jun, Y. Kastumata, J. Kauwe, P. G. Kehoe, L. Kilander, A. K. Ståhlbom, M. Kivipelto, A. Koivisto,
1072 J. Kornhuber, M. H. Kosmidis, W. A. Kukull, P. P. Kuksa, B. W. Kunkle, A. B. Kuzma, C. Lage, E. J. Laukka, L.
1073 Launer, A. Lauria, C.-Y. Lee, J. Lehtisalo, O. Lerch, A. Lleó, W. Longstreth, O. Lopez, A. L. de Munain, S. Love,
1074 M. Löwemark, L. Luckcuck, K. L. Lunetta, Y. Ma, J. Macías, C. A. MacLeod, W. Maier, F. Mangialasche, M.
1075 Spallazzi, M. Marquié, R. Marshall, E. R. Martin, A. M. Montes, C. M. Rodríguez, C. Masullo, R. Mayeux, S. Mead,
1076 P. Mecocci, M. Medina, A. Meggy, S. Mehrabian, S. Mendoza, M. Menéndez-González, P. Mir, S. Moebus, M. Mol,
1077 L. Molina-Porcel, L. Montréal, L. Morelli, F. Moreno, K. Morgan, T. Mosley, M. M. Nöthen, C. Muchnik, S.
1078 Mukherjee, B. Nacmias, T. Ngandu, G. Nicolas, B. G. Nordestgaard, R. Olaso, A. Orellana, M. Orsini, G. Ortega, A.
1079 Padovani, C. Paolo, G. Papenberg, L. Parnetti, F. Pasquier, P. Pastor, G. Peloso, A. Pérez-Cordón, J. Pérez-Tur, P.
1080 Pericard, O. Peters, Y. A. L. Pijnenburg, J. A. Pineda, G. Piñol-Ripoll, C. Pisanu, T. Polak, J. Popp, D. Posthuma, J.
1081 Priller, R. Puerta, O. Quenez, I. Quintela, J. Q. Thomassen, A. Rábano, I. Rainero, F. Rajabli, I. Ramakers, L. M.
1082 Real, M. J. T. Reinders, C. Reitz, D. Reyes-Dumeyer, P. Ridge, S. Riedel-Heller, P. Riederer, N. Roberto, E.
1083 Rodriguez-Rodriguez, A. Rongve, I. R. Allende, M. Rosende-Roca, J. L. Royo, E. Rubino, D. Rujescu, M. E. Sáez,
1084 P. Sakka, I. Saltvedt, Á. Sanabria, M. B. Sánchez-Arjona, F. Sanchez-Garcia, P. S. Juan, R. Sánchez-Valle, S. B.
1085 Sando, C. Sarnowski, C. L. Satizabal, M. Scamosci, N. Scarmeas, E. Scarpini, P. Scheltens, N. Scherbaum, M.
1086 Scherer, M. Schmid, A. Schneider, J. M. Schott, G. Selbæk, D. Seripa, M. Serrano, J. Sha, A. A. Shadrin, O. Skrobot,
1087 S. Slifer, G. J. L. Snijders, H. Soininen, V. Solfrizzi, A. Solomon, Y. Song, S. Sorbi, O. Sotolongo-Grau, G. Spalletta,
1088 A. Spottke, A. Squassina, E. Stordal, J. P. Tartan, L. Tárraga, N. Tesí, A. Thalamuthu, T. Thomas, G. Tosto, L.
1089 Traykov, L. Tremolizzo, A. Tybjærg-Hansen, A. Uitterlinden, A. Ullgren, I. Ulstein, S. Valero, O. Valladares, C. V.
1090 Broeckhoven, J. Vance, B. N. Vardarajan, A. van der Lugt, J. V. Dongen, J. van Rooij, J. van Swieten, R.
1091 Vandenberghe, F. Verhey, J.-S. Vidal, J. Vogelsgang, M. Vyhalek, M. Wagner, D. Wallon, L.-S. Wang, R. Wang,
1092 L. Weinhold, J. Wiltfang, G. Windle, B. Woods, M. Yannakoulia, H. Zare, Y. Zhao, X. Zhang, C. Zhu, M. Zulaica,
1093 L. A. Farrer, B. M. Psaty, M. Ghanbari, T. Raj, P. Sachdev, K. Mather, F. Jessen, M. A. Ikram, A. de Mendonça, J.
1094 Hort, M. Tsolaki, M. A. Pericak-Vance, P. Amouyel, J. Williams, R. Frikke-Schmidt, J. Clarimon, J.-F. Deleuze, G.
1095 Rossi, S. Seshadri, O. A. Andreassen, M. Ingelsson, M. Hiltunen, K. Sleegers, G. D. Schellenberg, C. M. van Duijn,
1096 R. Sims, W. M. van der Flier, A. Ruiz, A. Ramirez, J.-C. Lambert, New insights into the genetic etiology of
1097 Alzheimer's disease and related dementias. *Nat Genet* **54**, 412–436 (2022).
1098 63. W. Huang, J. Zeng, L. Jia, D. Zhu, J. O'Brien, C. Ritchie, N. Shu, L. Su, Genetic risks of Alzheimer's by
1099 APOE and MAPT on cortical morphology in young healthy adults. *Brain Commun* **5**, fcad234 (2023).
1100 64. J. H. Lee, J. Ryan, C. Andreeescu, H. Aizenstein, H. K. Lim, Brainstem morphological changes in
1101 Alzheimer's disease. *Neuroreport* **26**, 411–415 (2015).
1102 65. P. Theofilas, A. J. Ehrenberg, S. Dunlop, A. T. Alho, A. Nguy, R. E. P. Leite, R. D. Rodriguez, M. B. Mejia,
1103 C. K. Suemoto, R. E. de Lucena Ferretti-Rebustini, L. Polichiso, C. F. Nascimento, W. W. Seeley, R. Nitirini, C. A.
1104 Pasqualucci, W. J. Filho, U. Rueb, J. Neuhaus, H. Heinsen, L. T. Grinberg, Locus coeruleus volume and cell
1105 population changes during Alzheimer's disease progression: a stereological study in human postmortem brains with
1106 potential implication for early-stage biomarker discovery. *Alzheimers Dement* **13**, 236–246 (2017).
1107 66. A. J. Ehrenberg, C. K. Suemoto, E. de Paula França Resende, C. Petersen, R. E. P. Leite, R. D. Rodriguez,
1108 R. E. de Lucena Ferretti-Rebustini, M. You, J. Oh, R. Nitirini, C. A. Pasqualucci, W. Jacob-Filho, J. H. Kramer, J. R.
1109 Gatchel, L. T. Grinberg, Neuropathologic Correlates of Psychiatric Symptoms in Alzheimer's Disease. *J Alzheimers
1110 Dis* **66**, 115–126 (2018).
1111 67. D. A. Koolen, R. Pfundt, K. Linda, G. Beunders, H. E. Veenstra-Knol, J. H. Conta, A. M. Fortuna, G.
1112 Gillessen-Kaesbach, S. Dugan, S. Halbach, O. A. Abdul-Rahman, H. M. Winesett, W. K. Chung, M. Dalton, P. S.
1113 Dimova, T. Mattina, K. Prescott, H. Z. Zhang, H. M. Saal, J. Y. Hehir-Kwa, M. H. Willemsen, C. W. Ockeloen, M.
1114 C. Jongmans, N. Van der Aa, P. Failla, C. Barone, E. Avola, A. S. Brooks, S. G. Kant, E. H. Gerkes, H. V. Firth, K.

- 1115 Öunap, L. M. Bird, D. Masser-Frye, J. R. Friedman, M. A. Sokunbi, A. Dixit, M. Splitt, M. K. Kukolich, J.
1116 McGaughran, B. P. Coe, J. Flórez, N. Nadif Kasri, H. G. Brunner, E. M. Thompson, J. Gecz, C. Romano, E. E.
1117 Eichler, B. B. de Vries, The Koolen-de Vries syndrome: a phenotypic comparison of patients with a 17q21.31
1118 microdeletion versus a KANSL1 sequence variant. *Eur J Hum Genet* **24**, 652–659 (2016).
- 1119 68. J. Xu, N. Liu, E. Polemiti, L. Garcia-Mondragon, J. Tang, X. Liu, T. Lett, L. Yu, M. M. Nöthen, J. Feng, C.
1120 Yu, A. Marquand, G. Schumann, Effects of urban living environments on mental health in adults. *Nat Med* **29**, 1456–
1121 1467 (2023).
- 1122 69. A. C. H. Chen, N. Manz, Y. Tang, M. Rangaswamy, L. Almasy, S. Kuperman, J. Nurnberger Jr, S. J.
1123 O'Connor, H. J. Edenberg, M. A. Schuckit, J. Tischfield, T. Foroud, L. J. Bierut, J. Rohrbaugh, J. P. Rice, A. Goate,
1124 V. Hesselbrock, B. Porjesz, Single-Nucleotide Polymorphisms in Corticotropin Releasing Hormone Receptor 1 Gene
1125 (CRHR1) Are Associated With Quantitative Trait of Event-Related Potential and Alcohol Dependence. *Alcoholism: Clinical and Experimental Research* **34**, 988–996 (2010).
- 1126 70. D. Blomeyer, J. Treutlein, G. Esser, M. H. Schmidt, G. Schumann, M. Laucht, Interaction between CRHR1
1127 Gene and Stressful Life Events Predicts Adolescent Heavy Alcohol Use. *Biological Psychiatry* **63**, 146–151 (2008).
- 1128 71. R. Daviet, G. Aydogan, K. Jagannathan, N. Spilka, P. D. Koellinger, H. R. Kranzler, G. Nave, R. R.
1129 Wetherill, Associations between alcohol consumption and gray and white matter volumes in the UK Biobank. *Nat Commun* **13**, 1175 (2022).
- 1130 72. A. Thompson, J. Cook, H. Choquet, E. Jorgenson, J. Yin, T. Kinnunen, J. Barclay, A. P. Morris, M.
1131 Pirmohamed, Functional validity, role, and implications of heavy alcohol consumption genetic loci. *Sci Adv* **6**,
1132 eaay5034 (2020).
- 1133 73. T. Chambers, V. Escott-Price, S. Legge, E. Baker, K. D. Singh, J. T. R. Walters, X. Caseras, R. J. L. Anney,
1134 Genetic common variants associated with cerebellar volume and their overlap with mental disorders: a study on
1135 33,265 individuals from the UK-Biobank. *Mol Psychiatry* **27**, 2282–2290 (2022).
- 1136 74. N. C. Andreasen, R. Pierson, The Role of the Cerebellum in Schizophrenia. *Biol Psychiatry* **64**, 81–88
1137 (2008).
- 1138 75. T. G. M. van Erp, D. P. Hobar, J. M. Rasmussen, D. C. Glahn, G. D. Pearlson, O. A. Andreassen, I. Agartz,
1139 L. T. Westlye, U. K. Haukvik, A. M. Dale, I. Melle, C. B. Hartberg, O. Gruber, B. Kraemer, D. Zilles, G. Donohoe,
1140 S. Kelly, C. McDonald, D. W. Morris, D. M. Cannon, A. Corvin, M. W. J. Machielsen, L. Koenders, L. de Haan, D.
1141 J. Veltman, T. D. Satterthwaite, D. H. Wolf, R. C. Gur, R. E. Gur, S. G. Potkin, D. H. Mathalon, B. A. Mueller, A.
1142 Preda, F. Macciardi, S. Ehrlich, E. Walton, J. Hass, V. D. Calhoun, H. J. Bockholt, S. R. Sponheim, J. M. Shoemaker,
1143 N. E. M. van Haren, H. E. H. Pol, R. A. Ophoff, R. S. Kahn, R. Roiz-Santiañez, B. Crespo-Facorro, L. Wang, K. I.
1144 Alpert, E. G. Jönsson, R. Dimitrova, C. Bois, H. C. Whalley, A. M. McIntosh, S. M. Lawrie, R. Hashimoto, P. M.
1145 Thompson, J. A. Turner, Subcortical brain volume abnormalities in 2028 individuals with schizophrenia and 2540
1146 healthy controls via the ENIGMA consortium. *Mol Psychiatry* **21**, 547–553 (2016).
- 1147 76. N. Okada, M. Fukunaga, K. Miura, K. Nemoto, J. Matsumoto, N. Hashimoto, M. Kiyota, K. Morita, D.
1148 Koshiyama, K. Ohi, T. Takahashi, M. Koeda, H. Yamamori, M. Fujimoto, Y. Yasuda, N. Hasegawa, H. Narita, S.
1149 Yokoyama, R. Mishima, T. Kawashima, Y. Kobayashi, D. Sasabayashi, K. Harada, M. Yamamoto, Y. Hirano, T.
1150 Itahashi, M. Nakataki, R. Hashimoto, K. K. Tha, S. Koike, T. Matsubara, G. Okada, T. G. M. van Erp, N. Jahanshad,
1151 R. Yoshimura, O. Abe, T. Onitsuka, Y. Watanabe, K. Matsuo, H. Yamasue, Y. Okamoto, M. Suzuki, J. A. Turner, P.
1152 M. Thompson, N. Ozaki, K. Kasai, R. Hashimoto, Subcortical volumetric alterations in four major psychiatric
1153 disorders: a mega-analysis study of 5604 subjects and a volumetric data-driven approach for classification. *Mol
1154 Psychiatry*, 1–11 (2023).
- 1155 77. Y. Jiang, C. Luo, J. Wang, L. Palaniyappan, X. Chang, S. Xiang, J. Zhang, M. Duan, H. Huang, C. Gaser, K.
1156 Nemoto, K. Miura, R. Hashimoto, L. T. Westlye, G. Richard, S. Fernandez-Cabello, N. Parker, O. A. Andreassen, T.
1157 Kircher, I. Nenadić, F. Stein, F. Thomas-Odenthal, L. Teutenberg, P. Usemann, U. Dannlowski, T. Hahn, D.
1158 Grotegerd, S. Meinert, R. Lencer, Y. Tang, T. Zhang, C. Li, W. Yue, Y. Zhang, X. Yu, E. Zhou, C.-P. Lin, S.-J. Tsai,
1159 A. L. Rodrigue, D. Glahn, G. Pearlson, J. Blangero, A. Karuk, E. Pomarol-Clotet, R. Salvador, P. Fuentes-
1160 Claramonte, M. Á. García-León, G. Spalletta, F. Piras, D. Vecchio, N. Banaj, J. Cheng, Z. Liu, J. Yang, A. S. Gonul,
1161 O. Uslu, B. B. Burhanoglu, A. U. Demir, K. Rootes-Murdy, V. D. Calhoun, K. Sim, M. Green, Y. Quidé, Y. C.
1162 Chung, W.-S. Kim, S. R. Sponheim, C. Demro, I. S. Ramsay, F. Iasevoli, A. de Bartolomeis, A. Barone, M.
1163 Ciccarelli, A. Brunetti, S. Cocozza, G. Pontillo, M. Tranfa, M. T. M. Park, M. Kirschner, F. Georgiadis, S. Kaiser, T.
1164 E. V. Rheenen, S. L. Rossell, M. Hughes, W. Woods, S. P. Carruthers, P. Sumner, E. Ringin, F. Spaniel, A. Skoch,
1165 D. Tomecek, P. Homan, S. Homan, W. Omilor, G. Cecere, D. D. Nguyen, A. Preda, S. Thomopoulos, N. Jahanshad,
1166 L.-B. Cui, D. Yao, P. M. Thompson, J. A. Turner, T. G. M. van Erp, W. Cheng, J. Feng, Two neurostructural
1167 subtypes: results of machine learning on brain images from 4,291 individuals with schizophrenia. *medRxiv*,
1168 2023.10.11.23296862 (2023).
- 1169 78. J. R. Glausier, D. A. Lewis, Dendritic spine pathology in schizophrenia. *Neuroscience* **251**, 90–107 (2013).
- 1170 79. S. Li, C. Ma, Y. Li, R. Chen, Y. Liu, L. P. Wan, Q. Xiong, C. Wang, Y. Huo, X. Dang, Y. Yang, L. Lv, X.
1171 Chen, N. Sheng, W. Li, X.-J. Luo, The schizophrenia-associated missense variant rs13107325 regulates dendritic
1172 spine density. *Transl Psychiatry* **12**, 1–12 (2022).
- 1173 80. E.-M. Stauffer, R. A. I. Bethlehem, L. Dorfschmidt, H. Won, V. Warrier, E. T. Bullmore, The genetic
1174

- 1176 relationships between brain structure and schizophrenia. *Nat Commun* **14**, 7820 (2023).
- 1177 81. S. H. Lee, S. Ripke, B. M. Neale, S. V. Faraone, S. M. Purcell, R. H. Perlis, B. J. Mowry, A. Thapar, M. E.
1178 Goddard, J. S. Witte, D. Absher, I. Agartz, H. Akil, F. Amin, O. A. Andreassen, A. Anjorin, R. Anney, V. Anttila, D.
1179 E. Arking, P. Asherson, M. H. Azevedo, L. Backlund, J. A. Badner, A. J. Bailey, T. Banaschewski, J. D. Barchas, M.
1180 R. Barnes, T. B. Barrett, N. Bass, A. Battaglia, M. Bauer, M. Bayés, F. Bellivier, S. E. Bergen, W. Berrettini, C.
1181 Betancur, T. Bettecken, J. Biederman, E. B. Binder, D. W. Black, D. H. R. Blackwood, C. S. Bloss, M. Boehnke, D.
1182 I. Boomsma, G. Breen, R. Breuer, R. Bruggeman, P. Cormican, N. G. Buccola, J. K. Buitelaar, W. E. Bunney, J. D.
1183 Buxbaum, W. F. Byerley, E. M. Byrne, S. Caesar, W. Cahn, R. M. Cantor, M. Casas, A. Chakravarti, K. Chambert,
1184 K. Choudhury, S. Cichon, C. R. Cloninger, D. A. Collier, E. H. Cook, H. Coon, B. Cormand, A. Corvin, W. H.
1185 Coryell, D. W. Craig, I. W. Craig, J. Crosbie, M. L. Cuccaro, D. Curtis, D. Czamara, S. Datta, G. Dawson, R. Day, E.
1186 J. De Geus, F. Degenhardt, S. Djurovic, G. J. Donohoe, A. E. Doyle, J. Duan, F. Dudbridge, E. Duketis, R. P.
1187 Ebstein, H. J. Edenberg, J. Elia, S. Ennis, B. Etain, A. Fanous, A. E. Farmer, I. N. Ferrier, M. Flickinger, E.
1188 Fombonne, T. Foroud, J. Frank, B. Franke, C. Fraser, R. Freedman, N. B. Freimer, C. M. Freitag, M. Friedl, L.
1189 Frisén, L. Gallagher, P. V. Gejman, L. Georgieva, E. S. Gershon, D. H. Geschwind, I. Giegling, M. Gill, S. D.
1190 Gordon, K. Gordon-Smith, E. K. Green, T. A. Greenwood, D. E. Grice, M. Gross, D. Grozeva, W. Guan, H. Gurling,
1191 L. De Haan, J. L. Haines, H. Hakonarson, J. Hallmayer, S. P. Hamilton, M. L. Hamshere, T. F. Hansen, A. M.
1192 Hartmann, M. Hautzinger, A. C. Heath, A. K. Henders, S. Herms, I. B. Hickie, M. Hipolito, S. Hoefels, P. A.
1193 Holmans, F. Holsboer, W. J. Hoogendoijk, J.-J. Hottenga, C. M. Hultman, V. Hus, A. Ingason, M. Ising, S. Jamain, E.
1194 G. Jones, I. Jones, L. Jones, J.-Y. Tzeng, A. K. Kähler, R. S. Kahn, R. Kandaswamy, M. C. Keller, J. L. Kennedy, E.
1195 Kenny, L. Kent, Y. Kim, G. K. Kirov, S. M. Klauck, L. Klei, J. A. Knowles, M. A. Kohli, D. L. Koller, B. Konte, A.
1196 Korszun, L. Krabbendam, R. Krasucki, J. Kuntsi, P. Kwan, M. Landén, N. Långström, M. Lathrop, J. Lawrence, W.
1197 B. Lawson, M. Leboyer, D. H. Ledbetter, P. H. Lee, T. Lencz, K.-P. Lesch, D. F. Levinson, C. M. Lewis, J. Li, P.
1198 Lichtenstein, J. A. Lieberman, D.-Y. Lin, D. H. Linszen, C. Liu, F. W. Lohoff, S. K. Loo, C. Lord, J. K. Lowe, S.
1199 Lucae, D. J. MacIntyre, P. A. F. Madden, E. Maestrini, P. K. E. Magnusson, P. B. Mahon, W. Maier, A. K. Malhotra,
1200 S. M. Mane, C. L. Martin, N. G. Martin, M. Mattheisen, K. Matthews, M. Mattingdal, S. A. McCarroll, K. A.
1201 McGhee, J. J. McGough, P. J. McGrath, P. McGuffin, M. G. McInnis, A. McIntosh, R. McKinney, A. W. McLean, F.
1202 J. McMahon, W. M. McMahon, A. McQuillin, H. Medeiros, S. E. Medland, S. Meier, I. Melle, F. Meng, J. Meyer, C.
1203 M. Middeldorp, L. Middleton, V. Milanova, A. Miranda, A. P. Monaco, G. W. Montgomery, J. L. Moran, D.
1204 Moreno-De-Luca, G. Morken, D. W. Morris, E. M. Morrow, V. Moskvina, P. Muglia, T. W. Mühlleisen, W. J. Muir,
1205 B. Müller-Myhsok, M. Murtha, R. M. Myers, I. Myint-Germeyns, M. C. Neale, S. F. Nelson, C. M. Nievergelt, I.
1206 Nikolov, V. Nimgaonkar, W. A. Nolen, M. M. Nöthen, J. I. Nurnberger, E. A. Nwulia, D. R. Nyholt, C. O'Dushlaine,
1207 R. D. Oades, A. Olincy, G. Oliveira, L. Olsen, R. A. Ophoff, U. Osby, M. J. Owen, A. Palotie, J. R. Parr, A. D.
1208 Paterson, C. N. Pato, M. T. Pato, B. W. Penninx, M. L. Pergadia, M. A. Pericak-Vance, B. S. Pickard, J. Pimm, J.
1209 Piven, D. Posthuma, J. B. Potash, F. Poustka, P. Propsting, V. Puri, D. J. Quested, E. M. Quinn, J. A. Ramos-Quiroga,
1210 H. B. Rasmussen, S. Raychaudhuri, K. Rehnström, A. Reif, M. Ribasés, J. P. Rice, M. Rietschel, K. Roeder, H.
1211 Roeyers, L. Rossin, A. Rothenberger, G. Rouleau, D. Ruderfer, D. Rujescu, A. R. Sanders, S. J. Sanders, S. L.
1212 Santangelo, J. A. Sergeant, R. Schachar, M. Schalling, Cross-Disorder Group of the Psychiatric Genomics
1213 Consortium, Genetic relationship between five psychiatric disorders estimated from genome-wide SNPs. *Nat Genet*
1214 **45**, 984–994 (2013).
- 1215 82. M. Madre, E. J. Canales-Rodríguez, P. Fuentes-Claramonte, S. Alonso-Lana, P. Salgado-Pineda, A.
1216 Guerrero-Pedraza, N. Moro, C. Bosque, J. J. Gomar, J. Ortíz-Gil, J. M. Goikolea, C. M. Bonnin, E. Vieta, S. Sarró, T.
1217 Maristany, P. J. McKenna, R. Salvador, E. Pomarol-Clotet, Structural abnormality in schizophrenia versus bipolar
1218 disorder: A whole brain cortical thickness, surface area, volume and gyration analyses. *NeuroImage: Clinical* **25**,
1219 102131 (2020).
- 1220 83. M. Canavan, M. J. O'Donnell, Hypertension and Cognitive Impairment: A Review of Mechanisms and Key
1221 Concepts. *Front Neurol* **13**, 821135 (2022).
- 1222 84. L. M. Jenkins, C. R. Garner, S. Kurian, J. P. Higgins, T. B. Parrish, S. Sedaghat, A. J. Nemeth, D. M. Lloyd-
1223 Jones, L. J. Launer, J. M. Hausdorff, L. Wang, F. A. Sorond, Cumulative Blood Pressure Exposure, Basal Ganglia,
1224 and Thalamic Morphology in Midlife. *Hypertension* **75**, 1289–1295 (2020).
- 1225 85. Y. Halchenko, K. Meyer, B. Poldrack, D. Solanki, A. Wagner, J. Gors, D. MacFarlane, D. Pustina, V.
1226 Sochat, S. Ghosh, C. Mönch, C. Markiewicz, L. Waite, I. Shlyakhter, A. De La Vega, S. Hayashi, C. Häusler, J.-B.
1227 Poline, T. Kadelka, K. Skytén, D. Jarecka, D. Kennedy, T. Strauss, M. Cieslak, P. Vavra, H.-I. Ioanas, R. Schneider,
1228 M. Pflüger, J. Haxby, S. Eickhoff, M. Hanke, DataLad: distributed system for joint management of code, data, and
1229 their relationship. *JOSS* **6**, 3262 (2021).
- 1230 86. C. C. Chang, C. C. Chow, L. C. Tellier, S. Vattikuti, S. M. Purcell, J. J. Lee, Second-generation PLINK:
1231 rising to the challenge of larger and richer datasets. *GigaSci* **4**, 7 (2015).
- 1232 87. C. Bycroft, C. Freeman, D. Petkova, G. Band, L. T. Elliott, K. Sharp, A. Motyer, D. Vukcevic, O. Delaneau,
1233 J. O'Connell, A. Cortes, S. Welsh, A. Young, M. Effingham, G. McVean, S. Leslie, N. Allen, P. Donnelly, J.
1234 Marchini, The UK Biobank resource with deep phenotyping and genomic data. *Nature* **562**, 203–209 (2018).
- 1235 88. M. Mills, N. Barban, F. C. Tropf, *An Introduction to Statistical Genetic Data Analysis* (The MIT Press,
1236 Cambridge, Massachusetts London, England, 2020).

- 1237 89. J. Graffelman, V. Moreno, The mid p-value in exact tests for Hardy-Weinberg equilibrium. *Statistical*
1238 *Applications in Genetics and Molecular Biology* **12** (2013).
- 1239 90. A. M. Dale, M. I. Sereno, Improved Localizadon of Cortical Activity by Combining EEG and MEG with
1240 MRI Cortical Surface Reconstruction: A Linear Approach. *Journal of Cognitive Neuroscience* **5**, 162–176 (1993).
- 1241 91. A. M. Dale, B. Fischl, M. I. Sereno, Cortical Surface-Based Analysis. *NeuroImage* **9**, 179–194 (1999).
- 1242 92. B. Fischl, M. I. Sereno, A. M. Dale, Cortical Surface-Based Analysis. *NeuroImage* **9**, 195–207 (1999).
- 1243 93. B. Fischl, M. I. Sereno, R. B. H. Tootell, A. M. Dale, High-resolution intersubject averaging and a
1244 coordinate system for the cortical surface. *Hum. Brain Mapp.* **8**, 272–284 (1999).
- 1245 94. B. Fischl, D. H. Salat, E. Busa, M. Albert, M. Dieterich, C. Haselgrove, A. van der Kouwe, R. Killiany, D.
1246 Kennedy, S. Klaveness, A. Montillo, N. Makris, B. Rosen, A. M. Dale, Whole Brain Segmentation: Automated
1247 Labeling of Neuroanatomical Structures in the Human Brain. *Neuron* **33**, 341–355 (2002).
- 1248 95. The 1000 Genomes Project Consortium, A. Auton, G. R. Abecasis, D. M. Altshuler, R. M. Durbin, G. R.
1249 Abecasis, D. R. Bentley, A. Chakravarti, A. G. Clark, P. Donnelly, E. E. Eichler, P. Flicek, S. B. Gabriel, R. A.
1250 Gibbs, E. D. Green, M. E. Hurles, B. M. Knoppers, J. O. Korbel, E. S. Lander, C. Lee, H. Lehrach, E. R. Mardis, G.
1251 T. Marth, G. A. McVean, D. A. Nickerson, J. P. Schmidt, S. T. Sherry, J. Wang, R. K. Wilson, R. A. Gibbs, E.
1252 Boerwinkle, H. Doddapaneni, Y. Han, V. Korchina, C. Kovar, S. Lee, D. Muzny, Jeffrey G. Reid, Y. Zhu, J. Wang,
1253 Y. Chang, Q. Feng, X. Fang, X. Guo, M. Jian, H. Jiang, X. Jin, T. Lan, G. Li, J. Li, Y. Li, S. Liu, X. Liu, Y. Lu, X.
1254 Ma, M. Tang, B. Wang, G. Wang, H. Wu, R. Wu, X. Xu, Y. Yin, D. Zhang, W. Zhang, J. Zhao, M. Zhao, X. Zheng,
1255 E. S. Lander, D. M. Altshuler, S. B. Gabriel, N. Gupta, N. Gharani, L. H. Toji, N. P. Gerry, A. M. Resch, P. Flicek, J.
1256 Barker, L. Clarke, L. Gil, S. E. Hunt, G. Kelman, E. Kulesha, R. Leinonen, W. M. McLaren, R. Radhakrishnan, A.
1257 Roa, D. Smirnov, R. E. Smith, I. Streeter, A. Thormann, I. Toneva, B. Vaughan, X. Zheng-Bradley, D. R. Bentley, R.
1258 Grocock, S. Humphray, T. James, Z. Kingsbury, H. Lehrach, R. Sudbrak, M. W. Albrecht, V. S. Amstislavskiy, T. A.
1259 Borodina, M. Lienhard, F. Mertes, M. Sultan, B. Timmermann, M.-L. Yaspo, E. R. Mardis, R. K. Wilson, L. Fulton,
1260 R. Fulton, S. T. Sherry, V. Ananiev, Z. Belaia, D. Beloslyudtsev, N. Bouk, C. Chen, D. Church, R. Cohen, C. Cook,
1261 J. Garner, T. Hefferon, M. Kimelman, C. Liu, J. Lopez, P. Meric, C. O'Sullivan, Y. Ostapchuk, L. Phan, S.
1262 Ponomarov, V. Schneider, E. Shekhtman, K. Sirotnik, D. Slotta, H. Zhang, G. A. McVean, R. M. Durbin, S.
1263 Balasubramaniam, J. Burton, P. Danecek, T. M. Keane, A. Kolb-Kokocinski, S. McCarthy, J. Stalker, M. Quail, J. P.
1264 Schmidt, C. J. Davies, J. Gollub, T. Webster, B. Wong, Y. Zhan, A. Auton, C. L. Campbell, Y. Kong, A. Marcketta,
1265 R. A. Gibbs, F. Yu, L. Antunes, M. Bainbridge, D. Muzny, A. Sabo, Z. Huang, J. Wang, L. J. M. Coin, L. Fang, X.
1266 Guo, X. Jin, G. Li, Q. Li, Y. Li, Z. Li, H. Lin, B. Liu, R. Luo, H. Shao, Y. Xie, C. Ye, C. Yu, F. Zhang, H. Zheng, H.
1267 Zhu, C. Alkan, E. Dal, F. Kahveci, G. T. Marth, E. P. Garrison, D. Kural, W.-P. Lee, W. Fung Leong, M. Stromberg,
1268 A. N. Ward, J. Wu, M. Zhang, M. J. Daly, M. A. DePristo, R. E. Handsaker, D. M. Altshuler, E. Banks, G. Bhatia, G.
1269 del Angel, S. B. Gabriel, G. Genovese, N. Gupta, H. Li, S. Kashin, E. S. Lander, S. A. McCarroll, J. C. Nemesh, R.
1270 E. Poplin, S. C. Yoon, J. Lihm, V. Makarov, A. G. Clark, S. Gottipati, A. Keinan, J. L. Rodriguez-Flores, J. O.
1271 Korbel, T. Rausch, M. H. Fritz, A. M. Stütz, P. Flicek, K. Beal, L. Clarke, A. Datta, J. Herrero, W. M. McLaren, G.
1272 R. S. Ritchie, R. E. Smith, D. Zerbino, X. Zheng-Bradley, P. C. Sabeti, I. Shlyakhter, S. F. Schaffner, J. Vitti, D. N.
1273 Cooper, E. V. Ball, P. D. Stenson, D. R. Bentley, B. Barnes, M. Bauer, R. Keira Cheetham, A. Cox, M. Eberle, S.
1274 Humphray, S. Kahn, L. Murray, J. Peden, R. Shaw, E. E. Kenny, M. A. Batzer, M. K. Konkel, J. A. Walker, D. G.
1275 MacArthur, M. Lek, R. Sudbrak, V. S. Amstislavskiy, R. Herwig, E. R. Mardis, L. Ding, D. C. Koboldt, D. Larson,
1276 K. Ye, S. Gravel, The 1000 Genomes Project Consortium, Corresponding authors, Steering committee, Production
1277 group, Baylor College of Medicine, BGI-Shenzhen, Broad Institute of MIT and Harvard, Coriell Institute for Medical
1278 Research, E. B. I. European Molecular Biology Laboratory, Illumina, Max Planck Institute for Molecular Genetics,
1279 McDonnell Genome Institute at Washington University, US National Institutes of Health, University of Oxford, W.
1280 T. S. Institute, Analysis group, Affymetrix, Albert Einstein College of Medicine, Bilkent University, Boston College,
1281 Cold Spring Harbor Laboratory, Cornell University, European Molecular Biology Laboratory, Harvard University,
1282 Human Gene Mutation Database, Icahn School of Medicine at Mount Sinai, Louisiana State University,
1283 Massachusetts General Hospital, McGill University, N. National Eye Institute, A global reference for human genetic
1284 variation. *Nature* **526**, 68–74 (2015).
- 1285 96. S. A. Lambert, L. Gil, S. Jupp, S. C. Ritchie, Y. Xu, A. Buniello, A. McMahon, G. Abraham, M. Chapman,
1286 H. Parkinson, J. Danesh, J. A. L. MacArthur, M. Inouye, The Polygenic Score Catalog as an open database for
1287 reproducibility and systematic evaluation. *Nat Genet* **53**, 420–425 (2021).
- 1288 97. D. Lai, E. C. Johnson, S. Colbert, G. Pandey, G. Chan, L. Bauer, M. W. Francis, V. Hesselbrock, C.
1289 Kamarajan, J. Kramer, W. Kuang, S. Kuo, S. Kuperman, Y. Liu, V. McCutcheon, Z. Pang, M. H. Plawecki, M.
1290 Schuckit, J. Tischfield, L. Wetherill, Y. Zang, H. J. Edenberg, B. Porjesz, A. Agrawal, T. Foroud, Evaluating risk for
1291 alcohol use disorder: Polygenic risk scores and family history. *Alcoholism: Clinical and Experimental Research* **46**,
1292 374–383 (2022).
- 1293 98. C. T. Butts, *Yacca: Yet Another Canonical Correlation Analysis Package* (2022; <https://CRAN.R-project.org/package=yacca>).
- 1294 99. G. Molenberghs, G. Verbeke, Likelihood Ratio, Score, and Wald Tests in a Constrained Parameter Space.
1295 *The American Statistician* **61**, 22–27 (2007).

1297 100. M. S. Mufford, D. van der Meer, T. Kaufmann, O. Frei, R. Ramesar, P. M. Thompson, N. Jahanshad, R. A.
1298 Morey, O. A. Andreassen, D. J. Stein, S. Dalvie, The Genetic Architecture of Amygdala Nuclei. *Biological
1299 Psychiatry* **95**, 72–84 (2024).

1300

1301

1302 Acknowledgments

1303

1304 The authors gratefully acknowledge the computing time granted by the JARA
1305 Vergabegremium and provided on the JARA Partition part of the supercomputer JURECA
1306 and the joint lab Supercomputing and Modeling for the Human Brain at
1307 Forschungszentrum Jülich.

1308

1309 Funding:

1310 Helmholtz Imaging grant (NimRLS, ZT-I-PF-4-010) (SP, FR, SE, KO, KP)
1311 Helmholtz Imaging grant (BrainShapes, ZT-I-PF-4-062) (SP, FR, SE, KO, KP)

1312

1313 Author contributions:

1314 Conceptualization: SP, SE, JW, KO, KP
1315 Methodology: SP, KO, KP
1316 Investigation: SP, KO, KP
1317 Visualization: SP
1318 Supervision: KO, KP
1319 Writing—original draft: SP, KO, KP
1320 Writing—review & editing: SP, FH, FR, SE, JW, KO, KP

1321

1322 **Competing interests:** Authors declare that they have no competing interests.

1323

1324 **Data and materials availability:** The primary data used in this study is from the UK
1325 Biobank. These data can be provided by UK Biobank pending scientific review and a
1326 completed material transfer agreement. Requests for the data should be submitted to the
1327 UK Biobank: www.ukbiobank.ac.uk. Specific UK Biobank data field codes are given in
1328 Materials and Methods. Other publicly available data sources and applications are cited in
1329 Materials and Methods. We will make our MOSTest summary statistics available online
1330 within the GWAS catalog: <https://ebi.ac.uk/gwas/>. We will further publish the FUMA
1331 results within the FUMA database.

1332 This study used openly available software and codes, specifically BrainPrint
1333 (<https://github.com/Deep-MI/BrainPrint>), MOSTest
1334 (<https://github.com/precimed/mostest>), FUMA (<https://fuma.ctglab.nl/>), MAGMA
1335 (<https://ctg.cnrc.nl/software/magma>, also implemented in FUMA), SCORE
1336 (<https://github.com/sriramlab/SCORE>), fastman (<https://github.com/kaustubhad/fastman>),
1337 ggseq3d (<https://github.com/ggseg/ggseg3d/>), circlize
1338 (<https://github.com/jokergoo/circlize>) and yacca (<https://cran.r-project.org/web/packages/yacca/>). We further used Affinity Designer for figure design.

1340